fluids

MDPI

Review

Recent Developments in Supercooled Large Droplet Research: Impact, Splashing, Surface Water Dynamics, and Ice Accretion

Yisen Guo [1], Yang Liu [2], Mark Sussman [3], Hui Hu [4] and Yongsheng Lian [1,*]

[1] Mechanical Engineering Department, University of Louisville, Louisville, KY 40292, USA; yisen.guo@gmail.com
[2] Mechanical Engineering Department, The City College of New York, New York, NY 10031, USA; yliu7@ccny.cuny.edu
[3] Department of Mathematics, Florida State University, Tallahassee, FL 32306, USA; sussman@math.fsu.edu
[4] Department of Aerospace Engineering, Iowa State University, Ames, IA 50011, USA; huhui@iastate.edu
* Correspondence: yongsheng.lian@louisville.edu

Abstract

Supercooled large droplets (SLDs), typically defined as droplets with diameters exceeding 100 μm, represent a significant meteorological hazard to aviation safety. Unlike conventional cloud-sized droplets, SLDs have higher inertia and can follow more ballistic trajectories, leading to impingement well aft of leading-edge ice protection systems. SLD icing is further complicated by high-speed splashing, secondary-droplet re-impingement, delayed solidification, and surface water runback. This paper reviews recent progress in understanding SLD impact, splashing, surface water transport, and ice accretion. The review discusses droplet impact on dry and wet surfaces, oblique impingement, ambient-air effects, non-instantaneous solidification, runback dynamics, and downstream ice growth. Emerging ice protection technologies, including superhydrophobic, lubricant-infused, and compliant surfaces, are also evaluated. By synthesizing these developments, this review connects fundamental droplet-impact physics with practical aviation icing challenges and mitigation strategies.

Keywords: supercooled large droplets; aircraft icing; droplet impact and splashing; surface water runback; ice protection systems

Academic Editor: Xuemin Ye

Received: 25 February 2026
Revised: 9 June 2026
Accepted: 14 June 2026
Published: 24 June 2026

1. Introduction

Aircraft icing remains a serious weather hazard to aviation safety [1]. Conventional icing scenarios typically involve cloud-sized supercooled droplets with a median volume diameter of 20 μm or less. Although these droplets exist in a meta-stable liquid state below freezing temperatures, their low inertia causes them to follow the aerodynamic streamlines closely. Consequently, their impingement is generally confined to a narrow region near the wing's leading edge. Upon impact, the low thermal mass of these droplets facilitates rapid solidification, resulting in ice accretions that tend to be conformal to the airframe geometry. Because this accumulation occurs primarily within the impingement limits, the resulting aerodynamic degradation is typically manageable for aircraft certified for flight into known icing conditions [1–4]. Furthermore, the physics governing accretion from these small droplets has been extensively characterized, allowing for robust prediction using current numerical and empirical models [5,6].

1.1. SLDs and Their Characteristics

Under meteorological conditions extending beyond standard certification envelopes, aircraft may encounter supercooled large droplets, a regime encompassing freezing drizzle and freezing rain. Defined by diameters exceeding 100 μm, SLDs exhibit distinct aerodynamic behavior governed by their higher inertia. First, unlike smaller cloud droplets, which readily follow the aerodynamic streamlines around the wings, SLDs are less responsive to the pressure gradients. Consequently, they deviate significantly from the local airflow, following more ballistic trajectories that extend the droplet impingement limit well aft of the stagnation region [5]. This allows SLDs to strike surfaces beyond the reach of conventional leading-edge ice protection systems (Figure 1), leading to the formation of hazardous, uncontrolled ice accretions [7,8]. More importantly, the hazard of SLDs does not arise from impingement location alone, but from the subsequent coupled evolution of splashing, liquid water redistribution, freezing, and downstream ice growth.

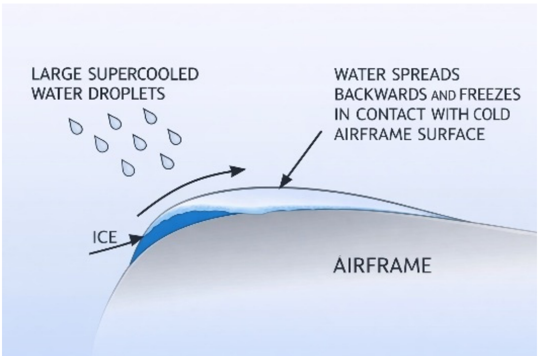

Figure 1. SLD icing on an airfoil surface.

Second, during SLD icing, the impinged droplets are more likely to splash into smaller droplets after impingement [9]. The splashed droplets can impinge back onto the wing surface further downstream beyond the regions protected by de-icing devices to cause uncontrolled ice accretion, which can lead to a significant decrease in lift and an increase in drag. In moderate to severe conditions, an airplane can become so iced up that continued flight becomes impossible [10]. Droplet splashing is an important component of SLD icing as it redistributes liquid mass and promotes downstream re-impingement, which must be considered together with non-instantaneous solidification, surface water runback, and subsequent ice accretion. Neglecting these in previous numerical simulations leads to poor agreement with experimental results [7,11,12]. While a number of droplet splashing models have been proposed [13,14], most of them were developed for normal impacts at relatively low droplet speeds, limiting their direct applicability to aircraft SLD icing, where impacts are often high-speed, oblique, and coupled with external airflow [15]. The characteristics of ambient air, which vary with the flight altitude of aircraft and can either suppress or exacerbate droplet splashing, were usually ignored [16–18].

Third, SLDs exhibit a distinct thermodynamic response upon impact compared to typical cloud-sized droplets. Unlike smaller droplets that possess low thermal mass and typically undergo instantaneous solidification upon contact, SLDs retain significant sensible heat and release substantial latent heat during the initial phase transition, thereby inhibiting immediate freezing. Consequently, only a small fraction of the droplet solidifies at the stagnation point. The remaining unfrozen liquid functions as runback water, driven aft by aerodynamic shear forces into regions often exceeding the coverage of leading-edge ice protection systems [5,19,20]. As it convects downstream, this surface water undergoes a complex morphological evolution, initially spreading as a continuous film before coalescing into discrete rivulets, which may ultimately disintegrate into isolated water beads

[11] (Figure 2). This runback redistribution is crucial to the distinction between SLD icing and conventional small-droplet icing, as it governs where and how liquid water ultimately freezes into glaze, mixed, or irregular ice accretions. Therefore, the key scientific challenge in SLD icing is not impact dynamics alone, but the coupling of impact, liquid transport, heat transfer, and phase change under aerodynamic conditions, which renders SLD ice accretion inherently unsteady, non-linear and computationally challenging to predict.

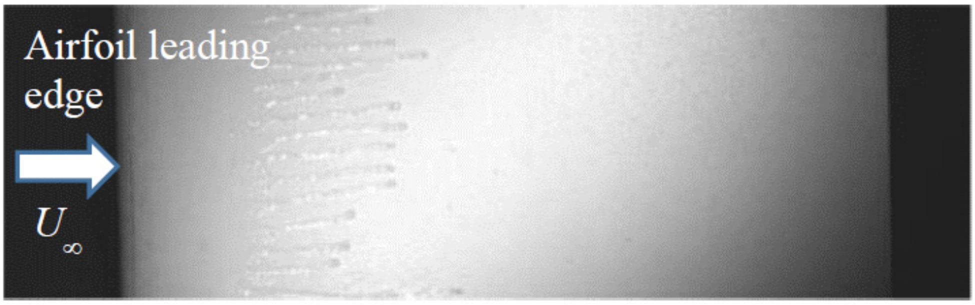

Figure 2. Experimental study to examine surface water runback over an ice-accreting airfoil [21].

Crucially, the surface water transport governs the local flow velocity and modulates the development of the thermal boundary layer over the accreting surface, thereby dictating the local heat transfer and subsequent freezing rates [22]. Unlike conformal ice profiles, this runback phenomenon fosters the growth of hazardous protuberances that penetrate the boundary layer and precipitate severe aerodynamic degradation. Historically, neglecting these runback dynamics in numerical simulations has resulted in significant discrepancies with experimental data [7,23,24]. Ultimately, the interaction between the boundary layer airflow, unfrozen surface water, ice substrate, and impinging droplets constitutes a highly coupled multiphase system, presenting a challenge for theoretical modeling and simulation.

1.2. SLD as an Aviation Hazard

SLD icing constitutes a critical meteorological hazard to aviation safety, implicated in multiple fatal accidents. Recent climatological assessments indicate that SLD encounters occur with significantly greater frequency than historically estimated [7,20,25]. The catastrophic potential of these conditions was tragically underscored by the crash of an ATR-72 in Roselawn, Indiana, on 31 October 1994, resulting in the loss of all 68 lives on board. The subsequent investigation by the National Transportation Safety Board (NTSB) identified the cause as ice forming aft of the de-icing system. The analysis confirmed that this anomalous accumulation was driven not by standard cloud-sized droplets, but by prolonged exposure to SLDs [20]. Consequently, establishing a robust fundamental understanding of SLD phenomenology is a prerequisite for the implementation of effective mitigation strategies. However, despite this urgency, current predictive capabilities for SLD ice accretion remain inadequate [7,11,26]. This persistent capability gap stems from the drastic disparity between the well-characterized physics of cloud-sized droplets and the complex, inertia-dominated microphysics governing SLD impact and solidification. In particular, the hazard is amplified by the coupled processes of splashing, downstream re-impingement, runback, and delayed freezing, which can generate ice accretion well beyond protected leading-edge regions.

1.3. Review Scope

Historically, icing research has predominantly focused on macroscopic observables, such as global ice shapes, impingement limits, and statistical water collection efficiencies.

https://doi.org/10.3390/fluids11070162

For example, Work and Lian reviewed the ice adhesion to solid substrates [27]. However, the governing micro-physical processes that dictate these outcomes, specifically SLD impact dynamics, rebounding, splashing, surface water runback, and the non-equilibrium freezing process, remain insufficiently characterized [7,11,12,28–33].

Recent experimental advances have also begun to narrow the gap between simplified laboratory studies and aircraft SLD icing conditions. In particular, recent icing wind tunnel investigations, including the vertical icing wind tunnel efforts by ONERA, have provided more realistic environments for examining high-speed SLD impact, splashing, surface water behavior, and ice accretion under aerodynamic flow. The ONERA icing wind tunnel, for example, enables experiments at Weber numbers on the order of 160,000, allowing detailed visualization and characterization of high-velocity SLD splashing on clean and iced substrates under conditions approaching real flight regimes [34] ONERA has also conducted high-speed SLD accretion tests at velocities up to 190 m/s and altitudes near 11,500 m, providing rare data on ice-thickness evolution and the sensitivity of accretion to droplet size, impact angle, temperature, and airflow conditions [35]. Complementary efforts such as the ONERA Research Icing Wind Tunnel have further demonstrated the ability to generate SLDs up to 300 μm and to reproduce realistic thermodynamic and aerodynamic environments for studying impact, runback, and accretion processes [36]. These studies are especially valuable because they move beyond isolated low-speed droplet impacts and offer stronger support for understanding SLD physics in conditions closer to those encountered in real flight.

To address this fundamental gap, this review provides a comprehensive synthesis of the recent progress in SLD micro-physics. The paper is organized as follows: Section 2 and Section 3 examine the fundamental mechanisms of droplet impact on dry and wet surfaces, respectively. Section 4 extends this analysis to complex, flight-relevant scenarios, including oblique impingement and multiple-drop interactions. Section 5 focuses on the coupled thermodynamic and surface water processes that control SLD ice accretion under aerodynamic conditions, while Section 6 reviews the efficacy of emerging ice protection technologies, including superhydrophobic and lubricant-infused surfaces, in mitigating SLD hazards.

2. Normal Drop Impact on Dry Surfaces

Although a normal impact on dry surfaces is an idealized configuration, it provides the baseline understanding of spreading, splash initiation, and secondary-droplet generation. However, direct extrapolation of these results to aircraft SLD icing should be made with caution, since practical icing conditions involve high-speed, oblique impacts, external airflow, evolving wet/iced substrates, and phase change.

2.1. Impact Outcomes

The impingement of a droplet on a flat, dry surface is governed by the competition between inertial, viscous, and capillary forces. Mundo et al. [14] experimentally delineated two primary outcomes: lower-inertia drops deposit on the surface to form a coherent liquid film, while higher-inertia drops splash, disintegrating into secondary droplets. They proposed the dimensionless parameter K to define the critical transition boundary between deposition and splashing, formulated as a function of the Ohnesorge (Oh) and Reynolds (Re) numbers:

$$K = OhRe^{1.25}$$

$$\mathrm{Re} = \frac{\rho D V_0}{\mu}$$

$$\mathrm{Oh} = \frac{\mu}{\sqrt{\rho \sigma D_0}}$$

where ρ, μ and σ represent the liquid density, viscosity, and surface tension, respectively, while D_0 and V_0 denote the droplet diameter and impact velocity. From this *K*-threshold it is easy to tell that inertial forces prompt splashing while viscous and capillary forces suppress splashing. Expanding on this binary classification, Rioboo et al. [37] identified six distinct impact regimes, ranging from deposition to complete rebound. These regimes (Figure 3) have been subsequently confirmed by others [38].

- **Deposition:** Occurs when a drop deforms and stays attached to the surface without breakup.
- **Prompt splash:** Typically associated with surface roughness, this regime is characterized by droplet ejection directly from the advancing contact line during the early spreading phase. Small finger-like jets form along azimuthal instabilities at the liquid edge, producing secondary droplets without any lift-off from the surface.
- **Corona splash:** In this regime, the spreading liquid lifts off from the surface to form a crown-like lamella (corona). The rim of this expanding sheet becomes unstable, leading to breakup into secondary droplets. Droplet formation is therefore governed by rim instability rather than direct contact-line dynamics.
- **Receding breakup:** A wetting phenomenon where some drops are left behind as the liquid retracts from its maximum radius.
- **Rebound and partial rebound:** Occurs when a receding phase is observed, depending on the maximum diameter reached and the receding contact angle.

Their study emphasized that beyond impact kinematics, surface properties such as wettability and roughness play a governing role in determining the outcome. Bartolo et al. [39] identified the jetting outcome, where a high-speed vertical jet shoots upwards from the center of the drop upon impact. This occurs on hydrophobic surfaces when the collapsing cavity focuses energy at the center. Tsai, P. et al. [40] shows that on textured surfaces, the outcome is not just splash or rebound, but can involve localized micro-splashing (fingering) at the pillar scale even if the macro-drop appears to spread. For SLD icing applications, these canonical outcomes are most useful as a mechanistic foundation rather than as direct predictors of aircraft icing behavior.

2.2. Non-Splashing Regimes: Spreading and Rebound

For non-splashing outcomes, including spreading, receding, and rebound, both analytical and numerical models have achieved relatively good predictive capability, particularly at moderate Weber numbers [41–44]. Early numerical work established that the rebound could be captured by solving the Navier–Stokes equations with the Marker-and-Cell method [45]. Later studies improved the treatment of free-surface deformation, contact-line motion, and dynamic contact-angle effects, enabling better prediction of maximum spreading diameter and oblique-impact behavior [46–48]. Across these studies, viscosity emerges as a key parameter after the initial inertia-dominated wetting stage, controlling energy dissipation, spreading time, and final droplet morphology. In SLD icing, however, the main importance of spreading and rebound lies not only in hydrodynamic prediction, but in how these processes determine liquid redistribution prior to freezing.

2.3. Splashing Regimes: Thresholds

Table 1 summarizes various models for drop splash threshold and splashed mass on dry surfaces. Most of the prominent models rely on the Weber number, Ohnesorge number and Reynolds number. These empirical models usually give accurate predictions for normal impacts [7]. It is worth mentioning that most threshold correlations summarized here were developed under low-speed, normal-impact, and non-icing conditions. While they are valuable for identifying general trends in splash initiation, their direct application to aircraft SLD icing is limited because they typically do not account for oblique impact, high-speed aerodynamics, substrate wetness evolution, or concurrent solidification.

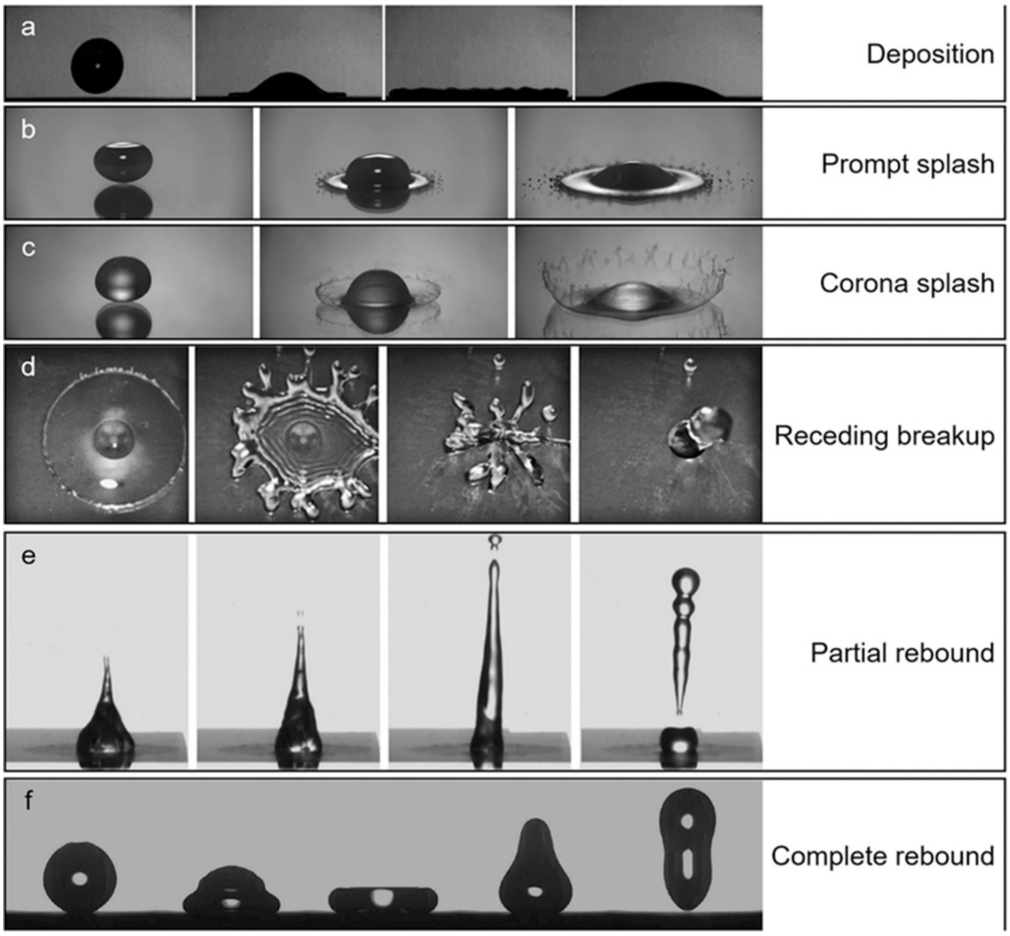

Figure 3. Distinct outcomes of drop impact on a dry surface [38]. (**a**) Deposition; (**b**) Prompt splash; (**c**) Corona splash; (**d**) Receding breakup (**e**) Partial rebound (**f**) Complete rebound.

Table 1. Drop splash threshold.

	Splash Threshold	Range of Variables and Properties
Mundo et al. [14,49]	$K = Re^{1/4}We^{1/2} > 57$ or $OhRe^{1.25} > 57.7$	Droplet Diameter Range $D_0 = 60 - 150$ μm Impact Velocity, $V_0 = 1.3 - 39.3$ m/s $K = 133.2 - 186.6$ $We = 620.1 - 1182.0$
Xu et al. [50]	$Oh = 3.60Re^{-0.75}$	$D_0 = 3.4 \pm 0.1$ mm $V_0 = 3.74 \pm 0.02$ m/s
Mandre and Brenner [51]	$V_0 \geq C\left(\frac{2\sigma^3}{\mu_g^2\rho D_0}\right)^{\frac{1}{4}}$; $C > 0.3$: interial asymptotic regime $C < 0.1$: surface − tension dominated	$\frac{St}{\delta} \approx 0.05 - 0.2$; with $\frac{St}{\delta} = \left(\frac{\rho_l VR}{\mu_g}\right)^{\frac{1}{3}}$

Schmehl et al. [52]	$S = \frac{1}{24}Re^{0.162}We^{0.419}$	
Vander Wal et al. [53]	For dry surface: $\sqrt{Ca} > 0.35$ For wet surface: $\sqrt{We} > 20$ $Oh \times Re^{0.609} > 0.85$: Dry Surface $Oh \times Re^{1.17} > 63$: thin film	$V_0(\text{m/s}) = 2.17{\sim}4.22$ $We = 127{\sim}1420$ Re = 988 ~ 13,900 Ca = 2.91~62.0 μ (cp): 0.409~2.95 σ(dynes/cm): 20.1~72.8
Stow and Hadfield [13]	$Oh_{\text{splash}} = 192Re^{-1.225}$	$1.4\ \text{mm} < D_0 < 4.4\ \text{mm}$ V_0: 2.1~12.41 m s^{-1}
Palacios et al. [54]	$We_c = 26.2Re^{0.433} + 9.96 \times 10^6 Re^{-1.65}$	$1.6 \le D \le 3.8$ mm $0.5 \le U \le 4.75$ m s^{-1} $786 \le \rho \le 1175$ kg m^{-3} $0.52 \le \mu \le 20.42$ mPa s $20.5 \le \sigma \le 70.8$ mN m^{-1} $100 \le Re \le 20{,}000$ $16 \le We \le 2000$
Walzel [55] and Schmidt and Knauss [56]	$We \times Oh^{-2.8} > 7.9 \times 10^{10}$ $57.7 = OhRe^{\frac{5}{4}}$	
Hardalupas et al. [57]	$Oh \times Re^{1.2} > 90$	$160 < D_0 < 230$ µm $58 < \sigma < 73$ mN/m $0.0010 < \mu < 0.0024 \frac{\text{kg}}{\text{m s}}$ $6 < V_0 < 13$ m/s
Cossali et al. [58]	$Oh \times Re^{1.25} > 119.23$	$2 \times 10^2 < We < 1.6 \times 10^3$ $2.2 \times 10^{-3} < Oh < 0.141$ $8 \times 10^{-2} < \delta_{film} < 1.2$
Range and Feuillebois [59]	$We > We_{crit}(\approx 310)$, $Oh_{crit} = We_{crit}^{\frac{1}{2}}Re^{-1}$	R_0: 1.94 ± 0.05 mm $172 \le We \le 1111$ $7315 \le Re \le 13{,}789$
Vander Wal et al. [60]	$Oh \times Re^{0.609} > 0.85$	D_0: 2.0 ± 0.06 mm V_0: 2.17~4.22 m/s μ: 0.409~3.34 cp σ: 20.1~72.8 dynes/cm ρ: 0.684~1.08 g/cm^3
Riboux and Gordillo [61]	$Oh_g We^{\frac{5}{6}}$ for low Oh limit $Oh_g Oh Re^{\frac{5}{4}}$ for high Oh limit	V_0: 1.29~2.28 ms^{-1} $3 \times 10^{-4} \le \mu \le 10^{-2}$ Pa s $17 \le \sigma \le 72$ mN m^{-1}
Roisman et al. [62]	$\frac{We}{1+0.24R'^{(\frac{1}{2})}} = 29\left(\frac{R_{pk}}{R_{sm}}\right)^{-0.68}$ R_{pk} is the average height and R_{sm} the average width of roughness element, and $R' = \rho R_{pk} U_0 \phi / \mu$	D_0: 1~3 mm V_0: 0~8 m/s μ: 1~523 mPa · s σ: 23~72.75 mN/m ρ: 786~1260 kg/m^3
Bird et al. [63]	$We^{\frac{1}{2}}Re^{\frac{1}{4}}\left(1 - \frac{3.5U_t}{U_n Re^{-\frac{1}{2}}}\right) > 127.0$, U_t and U_n are tangential and normal velocities	D_0: 1.76~3.4 mm U_n: 1~4 m/s U_t: 20~22.5 m/s ν: 1.2×10^{-6} m^{2}s^{-1} γ: 23 mN/m ρ: 790 kg/m^3
Hao [64]	$K \sim \log\left(\frac{R_a}{R_0}\right)$, R_a =arithmetic amplitude average roughness R_0= droplet radius	D_0: 2.3~3.8 mm V_0: 1~5.1 m/s μ: 1~1.81 mPa · s σ: 22.9~72.9 mN/m ρ: 791~998 kg/m^3
de Goede et al. [65]	$\beta \approx 2.22 \frac{\sqrt{\mu_g}}{\tan(\alpha)}(\rho R)^{\frac{1}{6}} \frac{v_{sp}^{\frac{5}{6}}}{\sigma^{(\frac{2}{3})}}$ Or in terms of splashing velocity,	V_0: 0.1~4.7 m/s μ: 0.89~2.85 mPa · s σ: 21.8 ~ 72.0 mN/m ρ: 789~997 kg/m^3

https://doi.org/10.3390/fluids11070162

	$v_s^{\frac{5}{6}} = \frac{\sigma^{\frac{2}{3}}\beta\tan(\alpha)}{2.22\sqrt{\mu_g}(\rho R)^{\frac{1}{6}}}$	
Almohammadi and Amirfazli [66]	$Ca - K_2R^{-\frac{3}{2}} > K_1$ and $Ca < K_3$ $K_1 = 0.06$ $K_2 = 6762$ $K_3 = 1.6$	D_0: 2.5 $\pm$ 0.1 mm V_0: 0.5 − 3.3 m/s μ: 1~100 cSt σ: 20~70.0 mN/m ρ: 813~1219 kg/m^3
Quetzeri-Santiago et al. [67]	$\beta = \frac{\left(1 + \left(\frac{R_{pk}}{R_{sm}}\right)\right)}{1 - \cos(\theta_{max})}$	D_0: 1.9 $\pm$ 0.1 mm (ethanol) D_0: 2.4 $\pm$ 0.1 mm (water) V_0: 1.38 − 2.98 m/s $1790 \leq Re \leq 7152$ $63.48 \leq We \leq 548$
Ashida et al. [68]	$OhRe^{\frac{5}{8}} > K_c$ for corona splash, $K_c = 0.207\left(\frac{\mu_l}{\mu_g}\right)^{\frac{3}{8}}$ $OhRe^{\frac{5}{4}} > K_p$ for prompt splash, $K_p = \left(649 + 3.76\left(\frac{R_a}{D}\right)^{-0.63}\right)^{\frac{5}{8}}$	D_0: 2.16~2.48 mm V_0: 4.2~33 m/s
Burzynski et al. [9]	$Oh < 0.0044,\ We \geq 34Re^{\frac{1}{4}}$	D_0: 2.0~4.0 mm V_0: 6 $\pm$ 26 m/s μ: 0.303~1.24 mPas σ: 22.55~72.75 mN/m ρ: 790~998 kg/m^3
Zhang et al. [69]	$ReOh^{1.3} = 3.8$ for $(Oh < 0.007)$ $(Re - 5.03Re^{0.67})Oh^{1.3}$ for $(Oh > 0.007)$	D_0: 3.7 $\pm$ 0.1 mm V_0: 1.4~5 m/s μ: 1~25.08 mPas σ: 58~72 mN/m ρ: 0.998~1.178 g/cm^3
Garci-Geijo et al. [70]	$We_c \approx \left(\frac{R\cos\theta_0}{\varepsilon}\right)^{\frac{3}{5}}$, ε substrate roughness	$We = 34$~391
Yang et al. [71]	$We = 5Re^{0.5} + 10^4Re^{-0.75}$	$We = 20$~550
Aksoy et al. [72]	$We = f(Re, \text{concentration})$	$10^2 < Re < 10^4$ $50 < We < 500$ particle-laden droplets
Liu et al. [73]	Revised Riboux and Gordillo's theory [61] with the consideration of surface temperature	D_0 = 2.5 mm V_0 = 3–7 m/s Ultracold surface up to −39 °C
Tian et al. [74]	$K_n > K_{90,cr}\sin^{0.23}\theta$ $K_n = Re_n^{0.5}We_n^{0.33}$ θ: impact angle	D_0 = 50 μm V_0 = 13–14 m/s
Yang et al. [75]	$P_cT_c^{-0.5}We_T = 0.285Re_T^{0.5}Pe^{0.5}$ $P_c = P/P_0$, $T_c = T/T_0$	D_0 = 2.48 mm V_0 = 1.4 to 2.8 m/s T = −15 °C to −35 °C
Foltyn et al. [76]	$We_{crit} = 0.08\left(\frac{hD_0}{w_1w_2}\right)^2 - 0.11\left(\frac{hD_0}{w_1w_2}\right) + 180$ w_1, w_2 are pillar width and length	Re = 1135 to 12,240 We = 80 to 1165

While numerous empirical models exist to predict the splashing threshold, their applicability to aviation icing depends on their behavior in the high-Reynolds-number regime typical of flight. Figure 4 compares the critical Ohnesorge number against the Reynolds number for eleven models. A distinct trend is evident across all models: the Oh_{crit} decreases dramatically as the Re increases up to Re≈2000. However, beyond $Re \approx 4000$ this rate of decrease slows significantly, and the curves begin to plateau. This transition reveals a shift in the dominant physics governing the splash.

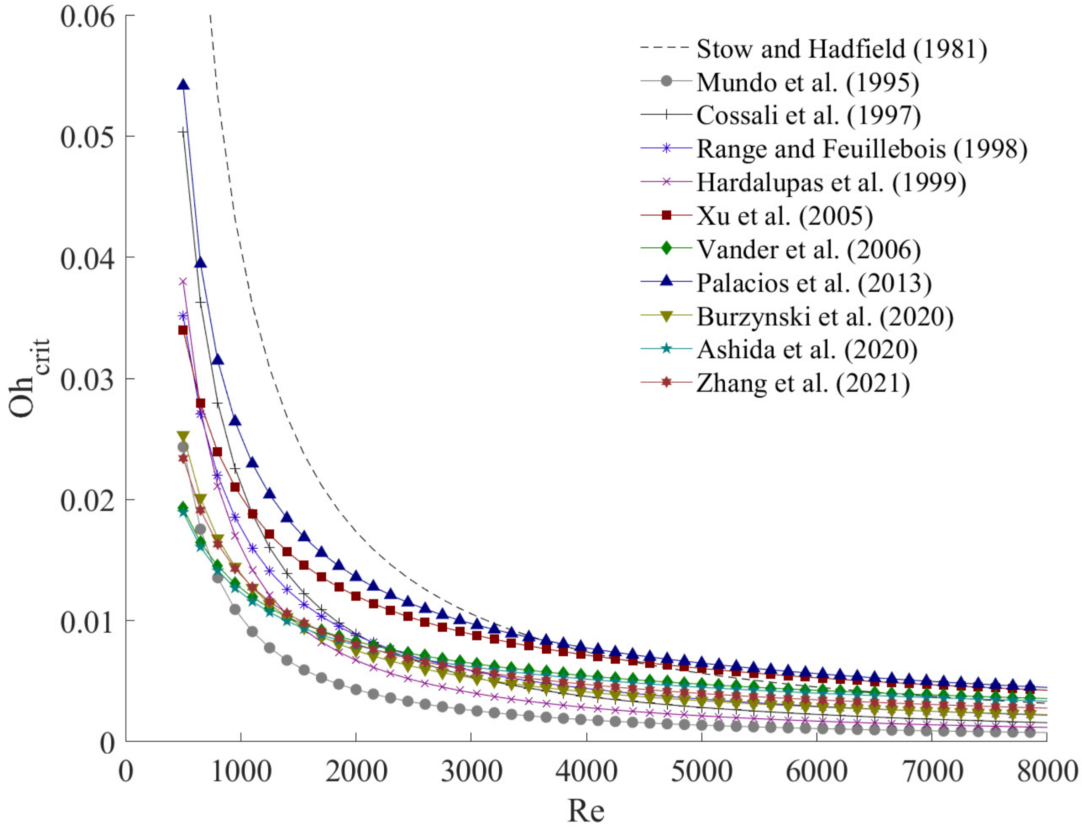

Figure 4. Comparison of different drop splashing on dry surface models based on the Ohnesorge (Oh) number vs. Reynolds (Re) number correlation. Figure is created using data from Stow and Hadfield [13], Mundo et al. [14], Cossali et al. [58], Range and Feuillebois [59], Hardalupas et al. [57], Xu et al. [16], Vander et al. [77], Palacios et al. [54], Burzynski et al. [9], Ashida et al. [68], Zhang et al. [69].

Low Re Regime (*Re* ≤ 2000): The threshold is highly sensitive to the Oh number, which represents the ratio of viscous forces to inertial and surface tension forces. In this regime, material properties, such as viscosity and surface tension, play a critical role in damping the impact energy and preventing splash.

High Re Regime (*Re* ≥ 4000): The curves flatten, indicating that the splashing threshold becomes less sensitive to changes in material properties and is instead dominated by the droplet's dynamic behavior (impact velocity and inertia). For SLD icing, which typically involves high-speed impacts corresponding to high Reynolds numbers, the inertial forces overwhelm the viscous dissipation capabilities of the fluid.

This apparent convergence suggests that some modern correlations may yield similar first-order trends at high Re; however, their predictive reliability under aircraft-relevant SLD conditions remains uncertain because most were calibrated under low-speed, normal-impact, non-freezing conditions. However, models like Stow and Hadfield [13] predict a significantly higher threshold at lower Re, which could lead to under-prediction of splashing mass loss in transitional flow regimes (e.g., near stagnation points or for smaller droplets). Therefore, for robust SLD icing prediction, models that capture this high-inertia asymptotic behavior are preferable, as they accurately reflect the dominance [78–80of dynamic inertial forces over material properties in the aviation environment.

Most classical splashing models in Table 1 were developed using experimental data where $V_0 < 10$ m/s, $Re < 10{,}000$, and $We < 2000$. In flight, the relative droplet velocity can reach tens to more than 100 m/s, although the effective normal impact component depends strongly on local airflow, surface curvature, and impact angle. A significant gap remains in the literature regarding high-inertia impacts relevant to aviation and wind turbine icing. While numerous studies have evaluated anti-/de-icing coatings [78–80], the majority were conducted at low impact speeds, conditions at least 1 to 2 orders of magnitude lower than those experienced in practical SLD icing events. Among the few who study high-speed drop impact on dry surfaces, Haller et al. [81] developed an analytical model for the high-pressure compression region of high-speed impacts, incorporating a real equation of state to resolve shock propagation. Guo and Lian et al. [82] conducted high-fidelity numerical investigations of droplet impingement at speeds greater than 50 m/s, identifying a critical dependency on ambient gas properties.

2.4. Differences Between Low-Speed and High-Speed Impacts

While the majority of fundamental drop impact studies are conducted at low impact velocities $V_0 < 10$ m/s, SLD icing involves velocities exceeding 50–150 m/s. Recent high-speed investigations, most notably by Burzynski et al. [9], highlight several physical regimes where low-speed empirical models fail to provide accurate predictions. The limitations of extrapolating low-speed data ($We < 3000$; $Re < 30{,}000$) to high-speed regimes ($We > 5000$; $Re > 50{,}000$) are quantified across multiple key physical dimensions.

2.4.1. Breakdown of Dimensionless Scaling and Thresholds

Traditionally, the splashing threshold is defined by a critical K parameter [49] or a β parameter [61]. At low speeds, a threshold of approximately $\beta \approx 0.14$ is widely accepted. However, at high-speed SLD conditions, this threshold is not constant. Burzynski et al. [9] demonstrated that the splashing threshold increases significantly with impact velocity. Furthermore, the relative importance of fluid properties shifts: at high speeds, the Reynolds number becomes the dominant factor over the Weber number.

2.4.2. Transition in Prompt Splash Mechanisms

In low-speed regimes, smooth surfaces typically suppress prompt splashing in favor of corona splashing. In contrast, at high speeds, prompt splash occurs regardless of surface finish. This is attributed to the emergence of Rayleigh–Taylor instabilities within the rapidly advancing liquid front.

2.4.3. Secondary Droplet Kinematics and Mass Balance

High-speed impacts produce extremely small secondary droplets. In the prompt splash regime, these droplets are rarely larger than 2% of the primary drop's diameter. While the mean velocity of these droplets seems to follow a universal trend regardless of speed. The total ejected volume increases with both velocity and viscosity at high speeds, suggesting a regime of total atomization that is not captured by linear extrapolations of low-speed mass-loss models.

2.5. Splashing Mechanisms

The fundamental mechanism initiating a splash, particularly in low-speed regions, remains a subject of debate [13,47,83–91]. Several mechanisms have been proposed to explain splash initiation, and their relative importance depends strongly on impact speed, surface roughness, ambient gas properties, and substrate condition. Rather than representing competing explanations for all cases, these mechanisms are best interpreted as regime-dependent pathways. Compressibility and shock-wave effects become important mainly at very high impact speeds; roughness-triggered contact-line instability is most relevant to prompt splash on rough or textured surfaces; and gas-mediated lamella lift is central to corona splash under sufficiently dense ambient gas. This regime-dependent interpretation is particularly important for SLD icing because aircraft impacts may transition among these mechanisms as velocity, impact angle, surface wetness, and air pressure vary.

Compressibility and Shock Waves: A prevalent theory attributes splashing to liquid compressibility and the geometric singularity formed by the parabolic interface at the moment of impact [81,92]. At very high impact velocities, the liquid cannot be treated as incompressible. A high-pressure shock wave forms upon contact. When this shock wave detaches from the contact line and moves up the droplet-free surface, the release of this high pressure drives a high-speed lateral jet (approximately 3–5 times the impact velocity), leading to splash and erosion. However, Mani et al. [93] argued that this compressible-liquid mechanism is insufficient to explain splashing at lower impact velocities.

Surface Roughness/Asperity Interaction (Prompt Splash): The mechanism for prompt splash involves the immediate ejection of droplets directly from the advancing liquid–solid contact line, rather than from the breakup of a spreading thin sheet. Several papers [13,37] established the causal link between surface roughness and the prompt splash. In these studies, roughness is typically described as the trigger that causes the advancing liquid sheet (lamella) to break up.

Specifically, Stow and Hadfield [13] identified that surface roughness determines the critical impact velocity (V_T) required for splashing. Their study utilized targets with a wide range of roughness, including polished stainless steel (R_a = 0.05 μm), various aluminum finishes (R_a from 0.05 μm to 3.10 μm) and a medium-rough target (R_a = 12 μm). They discovered a non-linear relationship between roughness and impact dynamics: V_T is highly sensitive to changes when $R_a < 1$ μm, decreasing by approximately 3 m/s for every 1 μm increase in roughness. However, for rougher surfaces where $R_a > 1$ μm, this dependence diminishes significantly. Ultimately, they concluded that roughness acts as an excitation for an instability in the developing watersheet. Interestingly, the scale of roughness required to influence this condition is considerably smaller than the characteristic thickness of the watersheet itself.

Building upon the foundational observations of Stow and Hadfield [13], Range and Feuillebois [59] refined the quantification of the prompt splashing threshold by transitioning from a velocity-based criterion to a dimensionless framework. Their experimental results for water–aluminum impacts confirmed the earlier findings while establishing a more generalized correlation: $We_c = a \log(R_0/R_a) + b$, where the critical Weber number We_c is linked to the ratio of drop radius to the surface roughness coefficient. Crucially, by utilizing various water–glycerin mixtures, they demonstrated that We_c is essentially independent of liquid viscosity, reinforcing the theory that the prompt splash is an inertia-dominated event triggered by surface geometry. They also observed that while the logarithmic relationship held across these varied targets, the non-universality of the coefficients a and b highlighted the subtle influence of specific liquid–surface interactions. Furthermore, they provided a mechanistic link to the instabilities suggested by Stow and Hadfield [13], observing that the number of perturbations on the spreading liquid rim is a direct function of the target's roughness.

Burzynski et al. [9] demonstrated that the prompt splash is governed by a Rayleigh–Taylor instability of the spreading lamella, making it primarily dependent on liquid properties, in contrast to the corona splash which is driven by aerodynamic effects of the surrounding gas. Latka et al. [18] experimentally demonstrated that this specific mechanism is driven by a critical interaction between surface roughness and ambient air pressure. Roughness acts as the primary promoter of the splash, but their study reveals that sufficient air pressure is required to enable the ejection: if the pressure falls below a specific threshold, the prompt splash mechanism is completely suppressed and the drop spreads smoothly. Latka's observation is consistent with Thoroddsen et al. [94] who observed prompt splash on smooth dry surfaces, indicating the roughness may not be solely responsible for prompt splash.

Aerodynamic Lift and Air Cushioning (Corona Splash): The corona splash is characterized by the lift-off of a liquid sheet from the substrate, forming a crown that subsequently disintegrates into secondary droplets. The initial lift-off is often attributed to aerodynamic forces [59,61] or kinematic discontinuities [95].

Other researchers posit that the surrounding gas is the dominant factor. Yarin [96] describes the mechanism as an aerodynamic interaction where the rapidly expanding lamella rides on a trapped cushion of air. As the air rushes out, it exerts an aerodynamic lift force on the leading edge; if this lift overcomes capillary retraction, the sheet levitates and breaks up [51]. This aerodynamic hypothesis is strongly supported by experimental work from Xu et al. [16] and Driscoll et al. [97], who demonstrated that lowering the ambient air pressure effectively suppresses splashing. Numerical simulations by Guo et al. [82] further validate the topology of the lifting sheet, though they did not observe the thin intervening air layer postulated by the aerodynamic models.

Mechanism of the Corona Splash: The corona splash is a complex, multi-stage phenomenon driven by significant gas–liquid interaction. Upon impact, the droplet forms a high-velocity liquid lamella that expands radially, displacing the ambient air. This interaction exerts an aerodynamic lift on the leading edge of the sheet. When the ambient gas pressure or density exceeds a critical threshold, the vertical force overcomes surface tension, causing the lamella to elevate from the substrate and form the characteristic crown-like structure. Liu et al. [98] proposed that a Kelvin-Helmholtz instability at the interface between the high-velocity liquid and the stationary ambient air is responsible for the initial destabilization. Their experiments demonstrated that suppressing the air layer effectively stabilizes the interface and prevents splashing.

The subsequent breakup of the elevated corona rim involves competition between inertial and capillary forces. Agbaglah and Deegan [99] resolved the debate regarding the governing instability of the rim. Their simulations revealed that while the Rayleigh–Taylor instability (caused by the radial deceleration of the rim) amplifies the growth rate of perturbations, it does not dictate their final spacing. Instead, the wavelength selection and final droplet size remain primarily governed by a Rayleigh–Plateau-like instability, where surface tension acts to minimize the surface area of the fluid rim.

Contact Line Instabilities and Fingering: As the liquid lamella expands radially across the substrate, the contact line frequently exhibits a morphological instability known as fingering. This phenomenon was first theoretically described by Allen [100], who attributed the formation of fingers to the Rayleigh–Taylor instability. Allen argued that the deceleration of the rapidly spreading liquid front creates an effective inertial force that drives the dense liquid into the lighter surrounding medium. Although the radial motion is damped by viscous forces, this deceleration is sufficient to destabilize the interface, causing azimuthal perturbations to grow into distinct fingers.

Subsequent experimental studies have validated this deceleration-driven mechanism. Mehdizadeh et al. [101] demonstrated that the wavelength of the instability aligns with predictions from linear Rayleigh–Taylor theory. Marmanis and Thoroddsen [102] established scaling laws relating the number of fingers to the Reynolds and Weber numbers, confirming the critical interplay of inertia and viscosity. It is important to distinguish this morphological change from splashing itself: while fingering acts as a precursor, it does not guarantee breakup. However, if the kinetic energy at the finger tips overcomes the capillary retraction force, the fingers will detach to form secondary droplets, transitioning the event into the prompt splash regime [103]. Recent experimental investigations further demonstrate that this fingering-to-droplet transition can be strongly modulated by interfacial forcing, which alters interfacial stresses and energy redistribution during impact [104]. For aircraft SLD icing, the practical importance of these splash mechanisms lies not only in secondary-droplet generation itself but also in how splashing redistributes water mass, alters local collection efficiency, and modifies subsequent freezing and accretion behavior.

2.6. Effect of Ambient Air Pressure

No splashing models in Table 1 take into account the effects of the surrounding air [88]. Burzynski and Bansmer [105] studied different surrounding gases such as Helium (He) and Ammonia (NH_3). For dry surfaces, they found that the most dominant gas property that affects the generation of secondary droplets due to splashing is the density, followed by the viscosity of the surrounding gas. They also noted that with the decrease in surrounding gas pressure, the splashing can be suppressed.

Xu et al. [16] and Latka et al. [18] have demonstrated that the ambient air plays a crucial role in determining the splashing behavior of droplets. They discovered that a reduction in air density or pressure can effectively suppress splashing. Xu et al. [16] showed that reducing ambient pressure can reduce splashing and splash can be completely suppressed in a low pressure environment. Another study also detected that corona splash can be suppressed by making tall pillars on the substrate surface even under normal atmospheric condition [50], as shown in Figure 5.

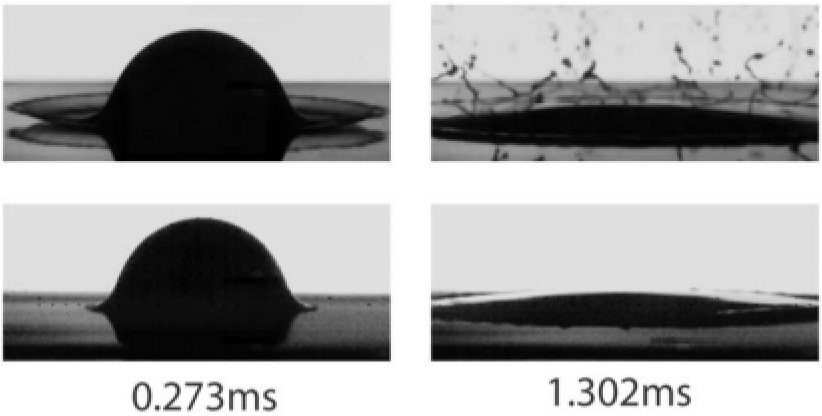

Figure 5. Drop impact at V_0 = 4.3 m/s and D_0 = 3.4 mm. A corona splash on a smooth surface (**top**) and splashing is seen to be completely suppressed on a surface consisting of pillars (**bottom**) [50].

Riboux and Gordillo [61] developed a theoretical model to predict droplet splashing while incorporating the effects of ambient air. Numerical simulations by Lian et al. [106] investigated the effect of air density on droplet impact. They found that a reduction in air density can lead to attenuation of the splash. Their simulation revealed that a thin film is formed upon contact of the droplet with a solid surface. The thin film moves at a low speed in the vicinity of the solid due to viscous effects, while it moves at a high speed away from the solid. The splashing is caused by the aerodynamic forces acting on the thin film. The thin film splashing is primarily initiated from the pre-existing liquid film on the solid surface, and the liquid content from the droplet sliding along it. These gas-phase effects are particularly relevant to SLD icing because aircraft motion and local aerodynamic conditions can strongly modify the gas–liquid interaction during impact, especially in high-speed and oblique impingement.

https://doi.org/10.3390/fluids11070162

2.7. Synthesis of Dominant Dry-Surface Splashing Mechanisms

The literature suggests that no single mechanism explains all splashing events. Instead, the dominant mechanism depends on the impact regime. For moderate-speed impacts on rough dry surfaces, prompt splash is most consistently associated with surface-roughness-triggered contact-line/lamella instability, with ambient gas pressure acting as an enabling condition rather than the primary trigger. For smooth or weakly rough surfaces at sufficiently high ambient pressure, corona splash is more consistently explained by gas-mediated lift of the expanding lamella, followed by capillary breakup of the raised rim. In contrast, compressibility and shock-wave mechanisms appear most relevant only in the very-high-speed regime, where liquid compressibility can no longer be neglected; they are unlikely to govern the lower-speed laboratory impacts often used to derive splash thresholds. Fingering should therefore be interpreted mainly as a precursor morphology that may lead to prompt splash if capillary retraction is overcome, rather than as an independent dominant mechanism in all cases.

Overall, dry-surface impact studies establish the fundamental mechanisms of spreading, rebound, prompt splashing, and corona splashing. However, their direct relevance to aircraft SLD icing is limited because dry, isothermal, normal-impact conditions exist only during the earliest stage of an icing encounter. For SLD applications, the greatest value of these studies lies in identifying the governing force balances and splashing mechanisms that must later be extended to wet, freezing, oblique, and high-speed conditions.

3. Normal Drop Impact on Wet Surfaces

In the context of aviation icing, the dry surface condition is transient, as the aircraft penetrates a cloud, the leading edge rapidly becomes wetted. Therefore, while these dry-surface thresholds are critical for the initial impingement, the wet-surface dynamics discussed in the following sections are more representative of the sustained ice accretion process, as they influence secondary-droplet generation, local water retention, and the downstream redistribution of liquid available for subsequent freezing.

The outcome of a droplet impacting a wetted surface is governed by the interplay of inertial and capillary forces; typically, high-momentum impacts result in splashing, while coalescence or deposition dominates in low-inertia regimes [96,107]. To characterize the substrate condition, the liquid layer is classified as either a film or a deep pool based on the non-dimensional parameter $\delta = h_0/D_0$, where h_0 is the liquid layer thickness and D_0 is the drop diameter. By convention, the layer is defined as a liquid film when $\delta < 1$ [58,108].

Figure 6 illustrates the initial conditions of a drop impacting a pre-existing liquid film of thickness. The post-impact hydrodynamics of a droplet impinging on a thin liquid film are dictated by the physical properties of the liquid phases, specifically density, viscosity, and surface tension, alongside the impact kinematics, including velocity and angle. These governing factors are conventionally consolidated into three dimensionless parameters: the Reynolds number, the Weber number, and the dimensionless film thickness.

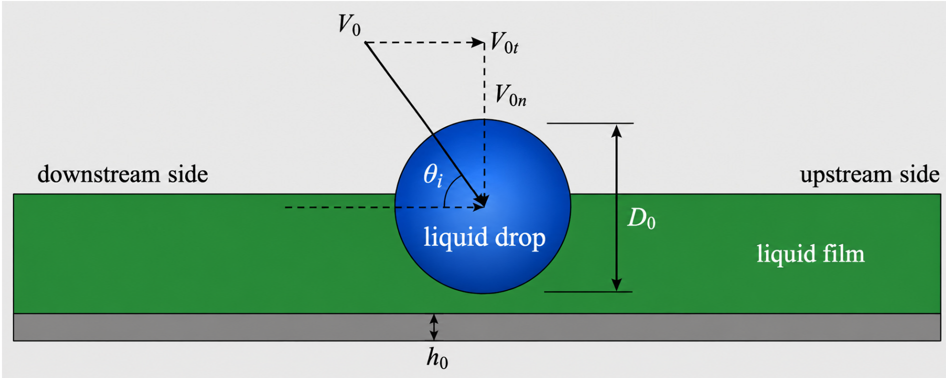

Figure 6. Illustration of drop impact on a thin film [109]. V_{0n} is the normal component of the velocity, θ is the impact angle, which dictates the distribution of energy between spreading and lateral jetting.

Experimental investigations [43,110,111] have classified the resulting motion into distinct regimes. In low-inertia regimes, the droplet deposits onto the liquid film without generating a crown. Conversely, high-inertia impacts induce the formation of a radially expanding crown, the breakup of which leads to splashing. This splashing phenomenon proceeds through a two-stage process [109]. The first stage is the ejecta formation in which a horn-shaped jet (ejecta sheet) emerges from the neck region and develops into a rising crown. The second stage is breakup in which instabilities along the crown rim cause the tip to disintegrate, ejecting secondary droplets.

Ribeiro et al. [112] identified six distinct outcomes for single-drop impacts on liquid films: deposition, fingering, prompt-splash, crown splash, jetting, and bubble encapsulation (Figure 7).

- **Low Energy**: The droplet merges with the film via spreading or deposition (Figure 7a)
- **Moderate Energy**: The drop may disintegrate immediately upon contact, resulting in a prompt splash, followed by the ejection of small droplets from the film periphery while the cylindrical crown sheet continues to rise (Figure 7b)
- **High Energy**: Inertia dominates, leading to crown splash, jetting, or rebound. Here, the fragmentation of the crown sheet into small droplets is driven by capillary instabilities (e.g., Rayleigh–Plateau) at the bounding rim (Figure 7c)

Early computational efforts to resolve drop impact on liquid films date back to Foote et al. [45], who solved the Navier–Stokes equations utilizing the Marker-and-Cell (MAC) method [113]. Subsequently, Bussmann et al. [47,88] employed the Volume of Fluid (VOF) method to simulate 3D impacts. Notably, these early models required the introduction of artificial perturbations to trigger splashing, highlighting the challenge of capturing natural instability growth in moderate-resolution simulations.

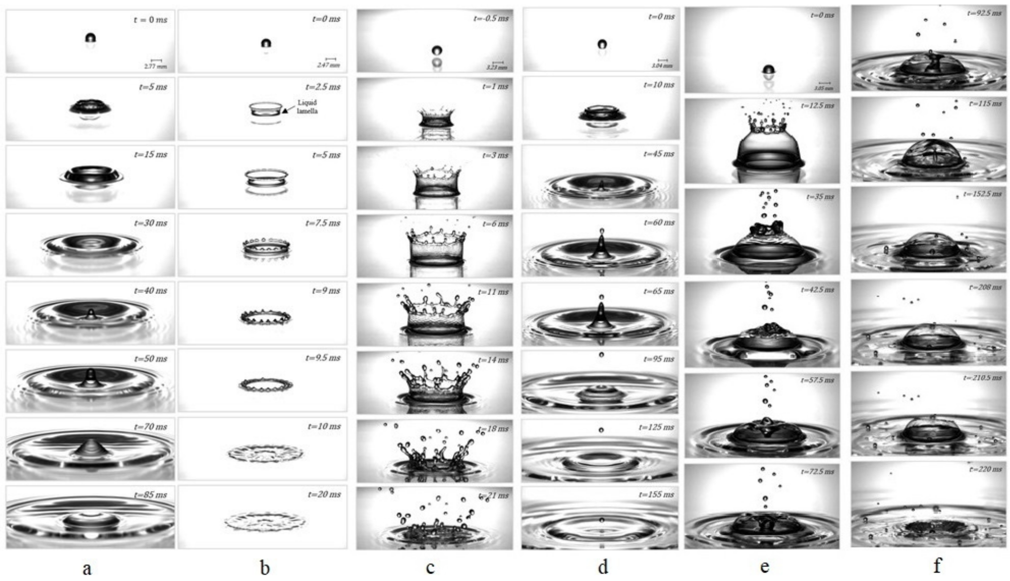

Figure 7. Ribeiro et al. [112] have shown the outcomes of drop impacts: (**a**) spreading; (**b**) fingering; (**c**) crown splash; (**d**) jetting; (**e**,**f**) splashing and bubble encapsulation, respectively.

3.1. Secondary Splashing Morphologies

In a focused investigation of impacts on thin liquid films, Zhu et al. [114] refined the morphological classification of secondary splashing. By mapping outcomes against the impact parameter K and dimensionless film thickness, they identified three distinct variations in the prompt splash:

(a) Active Delayed Splash: Observed at high impact energies and thinner films, this regime is driven by dominant inertial forces. During the crown's expansion phase, the kinetic energy of the developing fingers exceeds the restraining surface tension. Consequently, the fingers undergo rapid elongation and breakup via the Rayleigh–Plateau instability at the tips while the crown is still spreading radially.

(b) Passive Delayed Splash: Occurring at intermediate impact energies, this variation is characterized by a shift from inertial to capillary dominance. While initial fingers form, they lack sufficient momentum to break during expansion. As the crown reaches its maximum diameter and begins to recoil (retraction phase), surface tension pulls the fingers back. The breakup here is triggered by end-pinching.

(c) Prompt Splash without Delayed Splash: Found just above the splashing threshold, this outcome represents a state where viscous dissipation prevents droplet separation. Although rim instabilities generate visible fingers, the impact energy is insufficient to overcome surface tension during either the expansion or retraction phases. The fingers eventually retract and merge back into the pool without ejecting secondary delayed droplets.

Their regime map revealed a critical sensitivity to film thickness: increasing the film height was found to suppress the transition to active splashing by enhancing viscous dissipation at the impact crater, thereby requiring significantly higher impact velocities to achieve the same fragmentation outcome.

3.2. Kinematics of the Lamella and Crown Evolution

The kinematics of droplet impact on a liquid film can be understood as the coupled evolution of the spreading lamella, the rising crown, and the unstable rim. The basal lamella is primarily controlled by impact-driven radial momentum and is therefore less sensitive to Weber number than the upper rim dynamics [115]. In contrast, the rim reflects the competition between inertial stretching and capillary relaxation: higher Weber numbers generally produce thinner rims, more cusps, and a greater tendency toward ligament formation and secondary droplet ejection [95,116].

Crown propagation can be interpreted as a kinematic discontinuity governed strongly by film thickness, since thicker films entrain more liquid mass and reduce radial expansion velocity [43,117]. At higher impact energies, ejecta sheets, rim rupture, and slingshot-like droplet ejection provide additional atomization pathways [87,115,118–124]. For SLD icing, these crown and rim dynamics are important because they control both secondary-droplet production and the redistribution of liquid water available for downstream freezing.

3.3. Parametric Effects on Morphology

In this section, we examine how isolated physical parameters influence droplet impact on wetted surfaces. Subsequently, we evaluate splashing thresholds, which emerge from the synergistic effects of multiple governing variables.

A: Effect of Film Thickness: Research [77,114,125] has established that thinner films promote the splashing regime (Figure 8). In these scenarios, the film provides the requisite liquid volume for corona development without offering sufficient depth to effectively dissipate the droplet's kinetic energy. Because the liquid layer is shallow, the impact energy is not absorbed by a bulk volume; instead, it is redirected into high-velocity radial and vertical expansion. This results in the following:

- Wider Secondary Sprays: Droplets are launched further from the impact center due to the lack of vertical momentum absorption.
- Jet Suppression: The crown collapse in thin films lacks the necessary inward momentum to form a central jet, as the proximity of the solid substrate restricts the radial inflow required for jet emergence.

As the film thickness increases, the fluid layer begins to act as a momentum sink. Rioboo et al. [126] noted that beyond a critical thickness, the bulk liquid increasingly absorbs the droplet's kinetic energy through viscous damping and subsurface cavity formation. This leads to a distinct shift in morphology:

- Splash Inhibition: The prompt lateral splash is suppressed as the impact energy is partitioned into the displacement of the surrounding bulk liquid.
- Central Jet Formation: Unlike thin films, thicker layers provide a sufficient reservoir of fluid. When the impact-induced cavity collapses, the convergence of this larger fluid volume provides the momentum necessary to shoot a prominent central jet upward.

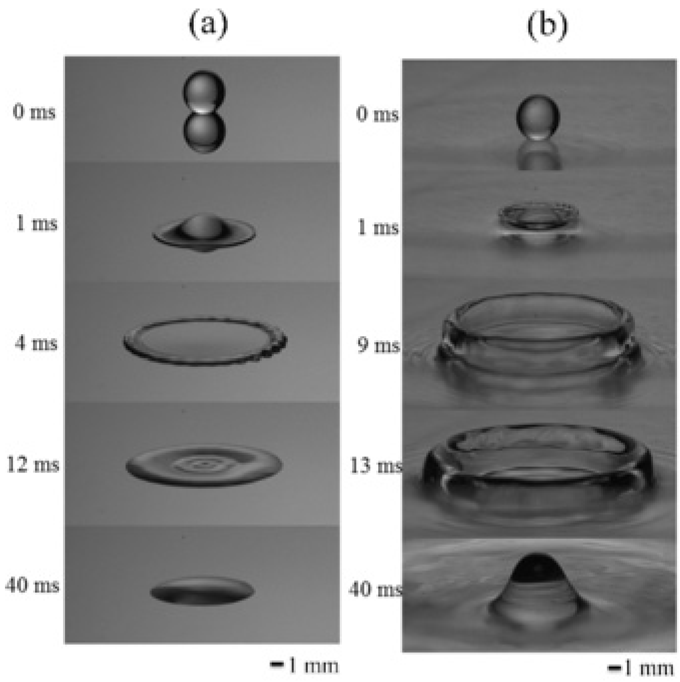

Figure 8. Impact of water drops on a (**a**) dry and (**b**) wet surface. Drop diameter is 3.2 mm and impact speed is 1.85 m/s [125].

When the droplet and film consist of different fluids, Chen et al. [127] identified a complex, dual role for film thickness: increasing the thickness of low-viscosity films promotes splashing due to Kelvin–Helmholtz-type instabilities at the interface, whereas increasing the thickness of high-viscosity immiscible films suppresses splashing by acting as an energy-absorbing soft solid

B: Effect of Surface Roughness: Substrate topography plays a critical role in modulating the splashing threshold. Vander Wal et al. [60] demonstrated that surface roughness can fundamentally alter impact dynamics. On smooth substrates, certain impacts may result in stable deposition; however, the same fluid-film system over a rough surface can exhibit both prompt and delayed splashing. This suggests that under these conditions, surface patterning can become the dominant control parameter, superseding both impact energy and intrinsic fluid properties. Zhu et al. [114] showed that roughness significantly enhances viscous dissipation at the solid–liquid interface. The increased hydrodynamic drag at the substrate curbs the radial expansion of the lamella base. Due to the conservation of mass, this restriction of radial flow forces the liquid to redirect vertically, resulting in a measurable increase in crown height compared to impacts on smooth surfaces.

Morphologically, surface roughness induces a hybrid splashing regime characterized by a non-axisymmetric crown. This structure exhibits circumferential unevenness, with thick, rib-like filaments extending from the base to the rim that provide structural support to the crown film. In this regime, droplet ejection is driven by dual mechanisms: an initial prompt breakup at the filament tips, followed by the Rayleigh–Plateau instability of the elongated filaments as the crown expands. Both mechanisms are driven by the kinematic discontinuities and broken symmetries imposed by the underlying surface texture.

C: Fluid Viscosity and Surface Tension: The outcome of a drop impact is primarily governed by the competition between inertial forces and the stabilizing effects of viscosity and surface tension. Generally, viscosity acts to dissipate kinetic energy and damp the growth of rim instabilities, thereby suppressing the transition to a splash. Similarly, surface tension provides a restorative force that opposes the expansion of the lamella. When the drop and film consist of different liquids, interfacial tension introduces an additional recoiling force, which typically results in smaller crown extensions.[128]

C1: Influence on Crown Dynamics and Splashing

The specific impact of viscosity on crown morphology has been well-documented. Rioboo et al. [126] established that increasing liquid viscosity significantly raises the energy threshold required for the crown-to-splash transition by damping the instabilities that lead to finger formation on the crown rim. Vander Wal et al. [60] further noted that viscosity and surface tension exert similar influences on the resulting spray, specifically regarding the size and number of secondary droplets. In cases of extreme viscosity, Kittel et al. [129] observed that droplets may bypass crown formation entirely, undergoing simple spreading instead. Conversely, low-viscosity wall films have been shown to facilitate rapid crown development and subsequent corona splash.

C2: Effects on Ejecta and Neck Mechanics

Viscosity also dictates the behavior of the liquid during the earliest stages of impact. According to Thoroddsen [118] and Josserand and Zaleski [110], the speed of the intact ejecta sheet decreases as viscosity increases. Josserand and Zaleski [110] highlighted that viscosity is a dominant factor in the neck region, where it dictates the initial width of the ejecta sheet that eventually evolves into the crown wall.

C3: The Interplay of Viscosity and Film Thickness

The relative importance of viscosity changes depending on the impact surface. While viscosity primarily dictates impact outcomes on dry surfaces, it is often superseded by film thickness as the dominant variable when a liquid layer is present [60]. However, this dominance is regime-dependent; Wang and Chen [130] discovered that for extremely thin films ($\sigma < 0.1$) the splashing threshold becomes largely insensitive to film thickness, placing the focus back on fluid properties.

C4: Complexities in Multi-Liquid Impacts

When a droplet impacts a film of a different liquid, the interaction is further complicated by viscosity ratios and interfacial tension [127,129,131,132]. Research by Bernard et al. [133] indicates that a high viscosity ratio (droplet is more viscous than the film) can lead to a two-stage crown morphology with the wall-film liquid concentrated at the upper part of the crown. Additionally, viscous losses during the extension phase can dissipate the initial energy, effectively preventing crown extension as much as capillary forces do. Regarding surface forces, a higher interfacial tension ratio acts as a recoiling force that reduces the duration of the ascending phase and results in smaller crown extensions. These interfacial forces also influence the splashing threshold. For instance, miscible liquids may require higher Weber numbers to initiate splashing due to the attenuation of the kinematic discontinuity at the droplet-film boundary.

3.4. The Splashing Threshold

While isolating individual parameters provides a fundamental understanding of fluid behavior, the transition from deposition to splashing is rarely the result of a single variable. Instead, the splashing threshold emerges from a complex interplay between inertial, viscous, and capillary forces. To characterize this boundary, researchers often synthesize these competing effects into dimensionless frameworks. By examining these combined metrics, we can define a critical limit that dictates the stability of the liquid crown across various film depths and fluid pairings.

Several semi-empirical correlations have been developed to predict the transition from deposition to splashing, as summarized in Table 2 [58,95,111,134]. However, a comparative analysis reveals significant divergence among these models, even for the fundamental case of water droplets impacting a thin liquid film (Figure 9). Notably, the model proposed by Yarin and Weiss [95] predicts a significantly higher threshold velocity for splashing than its counterparts, a discrepancy that becomes particularly pronounced at smaller droplet diameters.

Table 2. Selected splash threshold models for drop impact on liquid film.

	Splash Threshold
Yarin and Weiss [95]	$V_0^{5/8} D_0^{3/8} \rho^{3/8} \sigma^{-1/4} \mu^{-1/8} > 17$
Cossali et al. [58]	$Re^{0.4} We^{0.8} > 2100 + 5880\delta^{1.44}$ for $0.1 < \delta < 1$
Samenfink et al. [134]	$Re^{0.162} \cdot We^{0.419} > 24$
Deegan et al. [111]	$Re^{0.5} \cdot We > 26000$

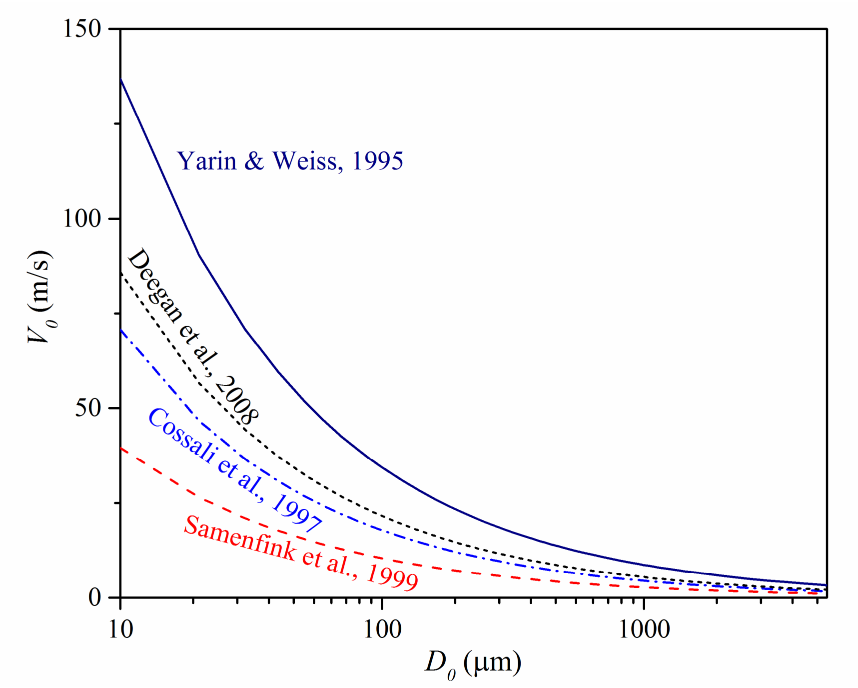

Figure 9. Selected splash threshold models for water drops impact on liquid films of δ = 0.1. The abscissa represents drop diameter and the ordinate represents the corresponding threshold velocity for splash. Figure is created using data from Yarin and Weiss [95], Deegan et al. [111], Cossali et al. [58], and Samenfink et al. [134].

Recent research has shifted away from simple curve-fitting toward deriving thresholds based on fundamental physical forces. Riboux and Gordillo [61] proposed a theoretical framework positing that splashing is driven by aerodynamic lift forces acting on the advancing lamella. They formulated a splashing parameter based on the ratio of these lift forces to restraining surface tension, suggesting that breakup occurs once this ratio exceeds a critical constant. While influential, the universality of this model has been questioned; for instance, Goede et al. [65] demonstrated that this lift-based criterion may not be applicable across diverse fluid types.

The threshold is further modulated by the motion of the target surface. Hao et al. [135] examined impacts onto moving substrates and determined that the critical splashing parameter is not static. They observed a reduction in the splashing threshold with increasing tangential velocity, implying that boundary layer shear or the relative motion of the substrate promotes interfacial instability. This finding is of particular relevance to aeronautical applications, as it suggests that splashing occurs more readily on an active wing than under static laboratory conditions.

3.5. Splashing Mechanisms on Wet Surfaces

The splashing mechanism on wetted surfaces is not a singular event but rather a hierarchy of fluid instabilities operating across distinct temporal and spatial scales. These transitions move from inertia-driven effects at the moment of impact to capillary-driven breakup during the final stages of atomization.

3.5.1. Stage I: Early Stage Ejecta and Inertial Instability

At the incipient moments of impact, particularly under high-inertia conditions, the interaction is dominated by a sharp kinematic discontinuity. Vander Wal et al. [77] elucidated that the pre-existing liquid film acts as an inertial barrier, inducing a rapid deceleration of the spreading lamella. This abrupt deceleration of the advancing fluid front generates a strong inertial force equivalent to an effective gravitational field acting across the liquid interface. Because the spreading liquid is effectively pushing against this deceleration into a stationary medium, the interface satisfies the classic criteria for Rayleigh–Taylor instability. Vander Wal et al. argued that this mechanism is primarily responsible for the prompt splash regime, driving initial azimuthal undulations along the nascent crown's rim. These undulations rapidly amplify into finger-like jets that subsequently fragment into fine secondary droplets before a stable corona is fully established.

Krechetnikov and Homsy [123] argued that the impulsive, shock-like acceleration favors the Richtmyer–Meshkov instability during these earliest stages, as RT requires more sustained acceleration than a typical impact shock provides.

3.5.2. Stage II: Intermediate Dynamics and Rim Instability

As the flow transitions to the crown formation phase (typically at moderate Weber numbers, We ≈ 200–1600), the governing physics shifts toward the geometry of the rim. Cossali et al. [58] demonstrated that while the bulk expansion of the crown is dictated by the initial kinematic discontinuity, the stability of the toroidal rim itself is capillary-driven.

The rim does not disintegrate spontaneously; instead, it undergoes a Rayleigh-type instability, forming cylindrical jets or fingers protruding from the rim [115]. Nikolopoulos et al. [120,136] proposed that this is a cooperative process: capillary instability governs the primary formation of these ligaments, followed by surface-tension-driven atomization.

3.5.3. Stage III: Final Atomization

The final stage of the splashing process, i.e., the actual detachment of secondary droplets, is universally governed by the Rayleigh–Plateau (RP) instability. Whether considering the fingers ejecting from a crown rim or the central column in deep-pool impacts, the physics of breakup remains consistent. Castillo-Orozco et al. [137] provided experimental confirmation of this mechanism on central jets, showing that surface tension drives the growth of capillary waves along the liquid column. When the amplitude of these waves grows sufficiently to bridge the jet radius, necking occurs, leading to pinch-off and the release of secondary droplets. This RP mechanism serves as the terminal step in the hierarchy, converting the ligaments generated by earlier RT or rim instabilities into the discrete droplets observed in the final splash spray.

This mechanism has been validated by Zhang et al. [138], who experimentally measured the spectrum of perturbations on the rim of a crown splash. Their results showed excellent agreement with the theoretical wavelength predicted by the Rayleigh–Plateau mechanism, confirming that the rim breakup is fundamentally a capillary-driven process. Other studies [120–122] attribute the breakup of ejecta-derived ligaments to this same RP mechanism.

3.5.4. Kinematic Discontinuity and Crown Propagation

Beyond instabilities themselves, the propagation of the crown itself is modeled as a kinematic discontinuity. Trujillo and Lee [117], effectively aligning with Yarin and Weiss [95], described the crown as a propagating jump in velocity and height. Their analysis (Re = 500–5000) demonstrated that after an initial transient phase, crown propagation becomes independent of the upstream drop flow and is governed solely by the target film thickness. Thicker films increase the entrained mass, retarding radial velocity through momentum conservation. Roisman and Tropea [43] later confirmed that in high-velocity impacts, liquid inertia dominates this process, rendering viscous discrepancies between various models (e.g., Trujillo vs. Yarin) negligible.

3.6. Mass Loss

For SLD icing, mass loss due to splashing is not merely a hydrodynamic outcome but a direct pathway for downstream re-impingement and uncontrolled ice accretion beyond protected regions. The critical parameter for SLD icing simulations is the mass loss ratio ($R_m = m_s/m_0$, where m_s is the splashed droplet mass and m_0 is the impact drop mass), representing the fraction of the incoming droplet mass that is ejected. Wet surface splashing can result in much higher mass loss than dry surface splashing, especially at lower impact velocity (<10 m/s). This ejected mass does not vanish but re-enters the freestream, often re-impinging aft of the protected leading edge.

Figure 10 compares the mass loss from splashing on the wet surface as a function of the *K* value with existing empirical models. Although the models of Samenfink et al. [134] and Schmehl et al. [52] predict that splashing occurs at the same *K* value, the model of Samenfink et al. [134] predicts higher splashed mass than the model of Schmehl et al. [52]. Figure 10 also indicates that the numerical result of Guo et al. [82] matches well with the prediction of Honsek et al. [139], which predicts that splashing occurs at a much larger *K* value.

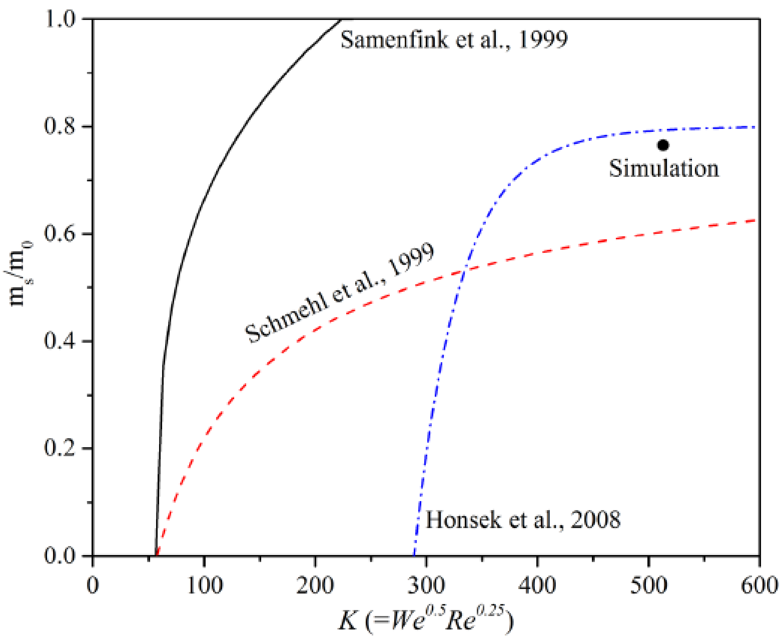

Figure 10. Comparison of mass loss from splashing with empirical models [82]. Figure is created using data from Samenfink et al. [134], Schmehl et al. [52], and Honsek et al. [139].

3.7. Effect of Ambient Air

Shetabivash et al. [140] numerically demonstrated that increasing ambient gas density retards the evolution of both crown radius and height due to increased aerodynamic drag. However, gas viscosity was found to have a negligible effect on the radial evolution rate.

Guo et al. [82] investigated the effect of surrounding gas on thin film splashing numerically. In their study, the impact of a 50 μm diameter water drop onto a uniform thickness water film with the impact velocity of 78 m/s was simulated and the film thickness was assumed to be 2 μm according to experiments by Zhang and Hu [141]. Thin film splashing is found to be less affected by ambient air than dry surface splashing but has a much larger splashed mass loss. In contrast to the dry surface cases, there is no significant difference in splashing suppression when the ambient air density is reduced. Nonetheless, the tip of the lamella moves slightly faster outward at lower air density than at higher air density. The lower-density air provides less resistance to the expanding lamella. Under aircraft icing conditions, these gas effects occur simultaneously with imposed external airflow and evolving surface wetness, making their role even more important than in static laboratory configurations.

A unified framework for gas–liquid coupling is provided by Riboux and Gordillo [61], who identify aerodynamic lift as the primary driver of splashing. In their model, splashing initiates when the vertical lift exerted on the liquid lamella's leading edge overcomes capillary retraction, preventing the liquid from re-attaching to the surface. This theory introduces a universal threshold parameter, $\beta \approx 0.14$, which successfully unifies the ambient pressure-dependency identified by Xu et al. [16] with the liquid property correlations of Mundo et al. [14]. By framing traditional empirical criteria as specific power-law limits of a global force balance, this framework provides the physical basis for scaling impact dynamics across varying gaseous atmospheres. For high-speed impact Burzynski et al. suggested $\beta \approx 0.19$ [9].

3.8. Synthesis of Dominant Wet-Surface Splashing Mechanisms

On wetted surfaces, dominance shifts both with time after impact and with film thickness. In the earliest stage, especially for high-inertia impacts onto thin films, splashing is governed by inertial destabilization of the ejecta/neck region. During the intermediate stage, when a crown forms, the dominant physics shifts to rim dynamics, where crown growth is set by impact kinematics and film thickness, while instability of the toroidal rim controls whether droplets are shed. In the final stage, secondary atomization is predominantly capillary-driven, with Rayleigh–Plateau-like breakup selecting droplet spacing and size. Increasing film thickness generally shifts the outcome away from prompt or active splashing and toward momentum absorption, splash suppression, and central jet formation, whereas increasing viscosity suppresses crown breakup by damping rim instability. Table 3 summarizes fluid behaviors and the associated dominated mechanisms for drop impact on both dry and wet surfaces.

In contrast to dry-surface impact, wet-surface impact is more representative of sustained SLD icing because incoming droplets often interact with pre-existing liquid films, runback water, or partially frozen substrates. Existing studies have clarified the roles of film thickness, crown formation, rim instability, and secondary atomization, but most remain limited to isothermal and low-speed conditions. For SLD icing, the key unresolved issue is how wet-surface splashing couples with aerodynamic shear, delayed freezing, and downstream re-impingement. This coupling directly controls liquid water redistribution and therefore strongly influences where ice forms beyond the protected leading-edge region.

Table 3. Likely dominant mechanism for drop impact on dry/wet surfaces.

Surface State	Observed Morphology	Likely Dominant Mechanism	Conditions Favoring Dominance	Conditions Suppressing It
Dry, rough	Prompt splash	Roughness-triggered contact-line/lamella instability	roughness, sufficient inertia, sufficient ambient gas pressure	smooth surface, low pressure, high viscosity
Dry, smooth	Corona splash	Gas-mediated lamella lift + rim breakup	high ambient pressure/density, high lamella speed, moderate/high We	reduced air pressure/density, stabilizing texture
Dry, very high speed	Erosive/high-speed jetting splash	Compressibility/shock-wave effects	very high impact speed	lower-speed lab regime
Wet, thin film	Prompt/active crown splash	Early inertial ejecta instability, then rim breakup	thin film, high inertia, low viscosity	thicker film, viscous damping
Wet, thicker film	Crown suppression/jetting	Momentum absorption by film, cavity collapse	thicker film, deeper liquid layer	very thin films
Wet, later times	Secondary atomization	Capillary breakup of rim/fingers	elongated rim/fingers, sufficient residual kinetic energy	strong viscous damping

4. Complex Impact Scenarios in Real SLD Icing

While Sections 2 and 3 summarize canonical droplet impact physics on dry and wet substrates, practical aircraft SLD icing occurs under substantially more complex conditions. In flight, SLDs rarely impinge as isolated, normal, low-speed droplets onto quiescent surfaces. Instead, they strike airplane surfaces at high speeds, often with strong tangential velocity components, under external aerodynamic shear. The surfaces may already be wet, partially frozen, or covered by ice roughness. Under such conditions, the droplet impact dynamics become a problem of coupled momentum, mass, and heat transport, in which impact angle, repeated interactions, liquid-film evolution, and freezing all affect how the surface water is redistributed and transported downstream along with the complex ice accretion.

In SLD icing, the key significance of complex impact scenarios is that they directly modify three controlling processes, i.e., the amount of water collected locally after impact, the fraction of water ejected or re-impinged downstream, and the evolution of the substrate on which subsequent droplets impact. These effects strongly influence runback extent, local freezing fraction, and the transition from initial impact to rime-, glaze-, or mixed-ice accretion. Therefore, oblique and repeated impacts should be considered as the central elements of aircraft SLD icing physics.

4.1. Oblique Drop Impingement

Oblique impact is especially relevant to aircraft icing because local collection angles on airfoils are rarely normal, particularly outside the stagnation region where many SLDs impinge. In practical SLD icing environments, the droplet momentum is partitioned into both normal and tangential components, and this redistribution alters not only spreading and splash onset but also downstream liquid transport and the spatial pattern of secondary-droplet generation. However, most of the existing literature has focused on normal impact conditions characterized by relatively low impact velocities (<10 m/s) and dimensionless film thicknesses δ greater than 0.1 [58,87,95,96,107,108,118,120,126,134,140,142,143]. In contrast, studies investigating high-speed oblique impact on thin liquid films remain rare.

Impact on Deep Pools (δ > 1): Among the few studies addressing oblique impact, early work by Ching et al. [144], Leneweit et al. [145] and Zhbankova and Kolpakov [146] focused on deep liquid pools in the non-splash regime. Leneweit et al. [145] observed that oblique impingement initially results in coalescence followed by interface depression. They identified a Weber number threshold of 10 governing the transition from convex capillary wave generation to the ejection of a lamella from the impact site. Conversely, Ching et al. [144] found that while droplet streams could bounce, single drops could not. They hypothesized that the disturbances on the liquid surface created by previous drops are necessary for bouncing, whereas a single drop dissipates most of its kinetic energy in crater formation, leaving insufficient energy for rebound. Although these studies were not conducted under icing conditions, they show that oblique momentum input can fundamentally alter interface deformation and energy partitioning even before splashing develops.

Studies on Moving and Oblique Surfaces: Several studies have utilized moving substrates to simulate oblique impact dynamics. Cheng and Lou [147] investigated oblique impact on both stationary and moving walls. They found that the stationary oblique wall experiments produced an asymmetric splash with an elliptical lamella, where crown fingers extended radially outward while spikes on the downstream side exhibited significant curvature. They developed a phase diagram correlating the moving wall speed with splashing phenomena. Similarly, Alghoul et al. [148] used a moving film setup to create an effective oblique impact angle. They reported an asymmetrical impact structure that became more symmetrical over time, while initially inclined in the direction of film motion. Notably, they observed that the height of the resulting jet increased with film height.

Hao and Green [135] further revealed that on a moving substrate, corona splash could be suppressed to a prompt splash. They also noted that reductions in ambient pressure could cause a transition from splashing to deposition. They hypothesized that aerodynamic lift forces acting on the lamella's leading edge are responsible for driving the separation that leads to splashing. More recently, Bao et al. [149] and Stober et al. [150] experimentally studied oblique droplet impacts on thin-wall films. Their findings are similar at the level of physical mechanisms, including asymmetric crowns, front-dominated splashing, and the importance of normal inertia and impact angle. Bao et al. provided thin film crown metrics and a K-number-based splashing threshold, while Stober et al. provided threshold formulas using impact angle and We for comparable oblique thin film impacts.

Numerical approaches have provided additional insights into the internal dynamics of oblique impact. Cheng and Lou [147] employed a Lattice Boltzmann model to study impacts at angles between 30° and 90°, observing a transition from crown splashing to single-sided splashing induced by cosine-wave perturbations on the drop surface. Guo and Lian [109] revealed that shallower impact angles lead to a smaller lamella on the downstream side and suppressed lamella development upstream (Figure 11). They attributed this to the origin of the liquid: the downstream lamella is formed primarily from the liquid film. Consequently, a thinner film results in a thinner and less stable lamella that breaks up earlier. Conversely, on the upstream side, increasing film thickness creates a thicker lamella with greater inertia. This increased inertia allows the lamella to resist aerodynamic drag more effectively, making the upward motion more prominent. These results are particularly relevant to SLD icing because they show that the combined effects of impact angle, film thickness, and aerodynamics can substantially change how liquid mass is redistributed over the surface after impact.

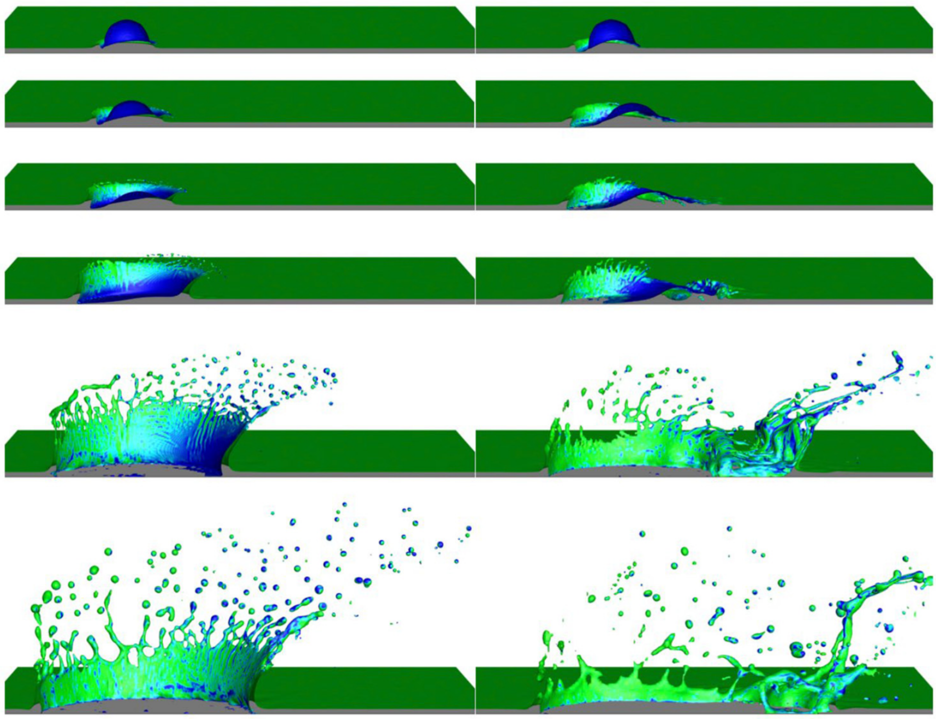

Figure 11. Oblique impact of a 41.3 μm-diameter water drop (Blue color) on a 5 μm-thick water film (Green color). (**Left**): Impact angle is 60° ($V_{0,normal}$= 53 m/s and $V_{0,tangential}$= 30.6 m/s). (**Right**): Impact angle is 30° ($V_{0,normal}$= 53 m/s and $V_{0,tangential}$= 91.8 m/s) [151].

Effect of Impact Angle and Fluid Properties: The influence of impact angle and fluid properties has been quantified in several extensive studies. Okawa et al. [152] analyzed over 500 cases, revealing that when the angle between the primary drop velocity and the surface normal was less than a critical threshold of 50°, increasing the impingement angle significantly increased the total mass of secondary drops. However, beyond this critical angle, secondary droplet formation ceased. Liang et al. [153] examined the role of surface tension and viscosity on inclined wetted substrates. They observed asymmetrical splashing and noted that increasing surface tension led to larger secondary droplet sizes. Furthermore, they identified a viscosity-dependent transition, where low-viscosity fluids exhibited prompt splashing while higher-viscosity fluids displayed delayed splashing.

Implications for SLD Icing: For aircraft icing applications, the importance of oblique impact extends far beyond splash morphology alone. In real icing environments, many impingement events occur away from the stagnation region, on curved or swept surfaces, and under local flow conditions that introduce substantial tangential velocity components. As a result, oblique impact is common not only on swept wings but also on downstream airfoil regions, rotating components, and surfaces already modified by runback water or evolving ice roughness. Under these conditions, models based solely on normal-impact correlations are unlikely to predict water collection efficiency, splashing loss, secondary-droplet transport, or runback-water redistribution accurately. A physically realistic description of SLD icing therefore requires explicit consideration of oblique impact, especially under high-speed conditions where tangential momentum and external airflow can strongly modify subsequent liquid transport, freezing, and ice accretion.

4.2. Multiple-Drop Impact

Repeated and interacting droplet impacts are highly relevant to aircraft SLD icing because flight surfaces are exposed to a continuous flux of droplets rather than isolated impacts. As a result, the local substrate evolves in time due to partial freezing, residual liquid accumulation, roughness growth, splashing deposits, and runback from previous impacts. This makes multiple-drop interaction a fundamentally important part of the coupled icing problem, since each new droplet encounters a surface that has already been modified by the preceding droplets.

Normal Impact: While single-drop studies provide fundamental insights, the practical reality of aircraft icing involves the impact of a continuous flux of droplets. In this regime, droplets rarely impact a quiescent surface. Instead, they impinge upon a dynamic liquid layer generated by previous impacts, leading to complex crown–crown interference phenomena. Roisman et al. [154] characterized these interactions on dry surfaces, identifying droplet spacing as the governing parameter for the resulting film flow.

Extending this to wetted surfaces, Raman et al. [155] and Li et al. [156] utilized the two-dimensional Lattice Boltzmann method to investigate the normal impingement of droplet pairs. Their simulations revealed that the collision of expanding crowns generates a distinct middle splash or central updraft. Raman et al. [155] found that the height of this central ejecta is inversely related to the dimensionless horizontal spacing. As drops impact closer, the constructive interference of the crowns intensifies. Li et al. [156] demonstrated that non-simultaneous impacts break the flow symmetry. They noted a complex non-linear relationship between droplet diameter and spacing, where the interaction intensity initially increases and then decreases as the horizontal distance grows, creating a specific window of maximum instability.

Oblique Interactions: In flight conditions, multiple impacts are almost invariably oblique. Guo and Lian [151] simulated high-speed droplet pairs (V_0 = 75 m/s) at impact angles of 30° and 60° to decouple the effects of tangential momentum (Figure 12). The low-angle (30°) case is dominated by horizontal shear. No downstream crown forms, and the upstream crown is stunted. The interaction between the two drops is relatively weak as the horizontal momentum convects the fluid downstream before significant crown–crown collision can occur. In the high-angle (60°) case the flow topology shifts drastically. The interacting lamellae twist into a complex S-shape, breaking up into elongated ligaments. The lower region of this S-structure moves horizontally downstream, while the upper region is driven upward, leading to a dual-mode breakup that significantly enhances secondary droplet production. These results highlight that repeated oblique impacts can generate flow structures and breakup pathways that are qualitatively different from those observed in isolated or normal-impact cases.

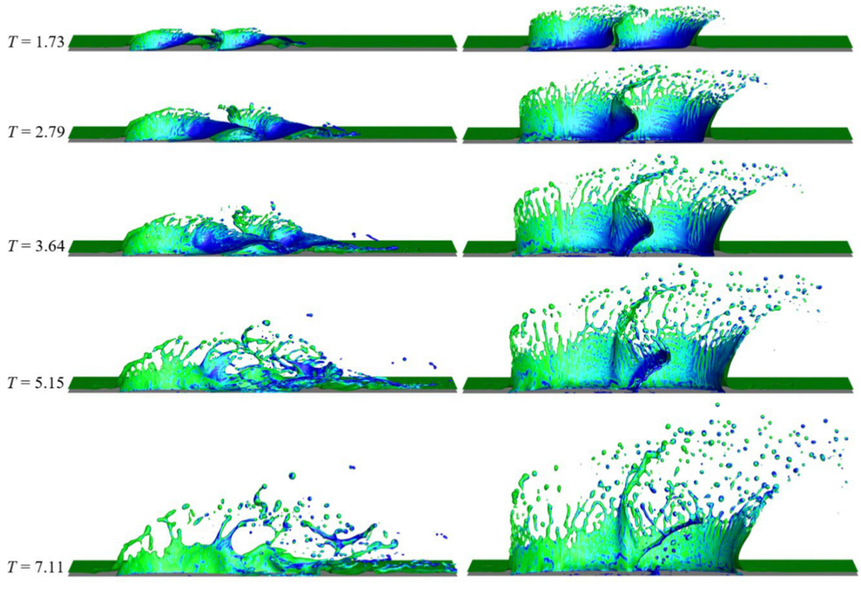

Figure 12. Comparison of high-speed drops impacts with 30° and 60° impact angles. Blue color is drop, green is water film. (D_0 = 41.3 μm, h_0 = 5 μm, V_0 = 75 m/s). (**Left**): θ = 30°; (**right**): θ = 60°[151].

Simultaneous vs. Successive Mechanisms: Liang et al. [153,157–159] conducted a series of studies distinguishing between simultaneous (spatial) and successive (temporal) multiple drop impacts. For simultaneous impacts they observed the formation of a central liquid sheet at the collision plane. Crucially, the splashing threshold is reduced in this regime due to the cracking or rupture of this central sheet. This rupture is initiated by surface tension forces but driven to violent splashing by gas-phase instabilities and the rapid expansion of trapped vapor bubbles on the inner crown wall.

For successive impacts, conversely, for drops impacting sequentially, the splashing threshold for the trailing droplet is higher (i.e., splashing is suppressed). This is attributed to the strong radial flow established by the leading drop, while the trailing drop impacts a fluid field that is already moving radially outward, which dissipates the impact energy and alters the kinematic discontinuity.

Thermal-Hydraulic Coupling: Liang et al. [153,157–159] also mapped the thermal footprint of these interactions. They observed that the impact region is significantly cooler than the surrounding film due to the impingement of supercooled mass. Interestingly, the temperature of the rising crown sheet was found to be much higher than that of the central liquid sheet. Since both structures are unsaturated, this thermal contrast serves as a passive tracer, confirming that the mass constituting the crown originates primarily from the warmer pre-existing liquid film, whereas the central sheet is composed largely of the cooler impinging droplet fluid. This uneven temperature distribution, coupled with localized hot spots where vapor bubbles form, creates thermal gradients that further influence the breakup instability.

Overall, the available literature indicates that canonical low-speed, normal-impact studies capture only part of the physics needed for aircraft SLD icing. A more realistic framework must account for high-speed, oblique, and repeated impacts together with airflow, liquid water transport, and phase change.

4.3. Synthesis of Flight-Relevant Impact Scenarios

Oblique and multiple-drop impacts constitute a critical transitional regime between canonical single-droplet impact studies and the complex, film-mediated interactions characteristic of SLD icing. Evidence shows that impact angle redistributes momentum between normal spreading and tangential transport, generating asymmetric crown structures, altered splashing thresholds, and shifted heat-flux distributions [150,160–162]. At the same time, repeated impacts or multi-drop interactions substantially modify the local hydrodynamic and thermal environment by building and reshaping liquid-film thickness, lowering splashing thresholds, promoting crown–crown collisions, and influencing secondary-droplet generation [163–166]. These interactions also alter local heat transfer behavior, producing thermal inhomogeneities and film-driven flow structures. Under cold-surface conditions, multi-drop impacts further change freezing modes and accelerate ice formation [167]. These mechanisms illustrate the strong thermo-fluid coupling that emerges under oblique and repeated impacts, aligning well with the physical processes underlying realistic SLD icing.

However, systematic data remain limited for high-speed oblique impacts on cold, wet, or ice-accreting surfaces under external airflow. Existing studies tend to isolate subsets of the problem; for example, oblique high-speed impacts onto gas-sheared or wavy liquid films reveal asymmetric crown evolution, furrow formation, and angle-dependent droplet dynamics but do not incorporate freezing or aerodynamic cooling effects [168,169]. Similarly, SLDs impacting freezing or partially frozen water films exhibit dendrite–crown interactions and strongly altered splashing behavior, yet these experiments occur in quiescent air and at modest impact angles [170]. Normal and oblique impacts on cold hydrophobic or superhydrophobic surfaces have been extensively simulated using VOFenthalpy, LBM, and multiphase models, confirming strong coupling between deformation, heat transfer, and phase change, but these simulations typically neglect crossflow aerodynamic shear and evolving ice morphology[171,172]. Even studies conducted in icing wind tunnels primarily resolve single-drop corona splashes or residual mass after impact rather than the detailed morphodynamics of oblique, repeated, or film-mediated events [173].

This gap is significant because aircraft SLD icing rarely consists of isolated normal impacts. Instead, droplets frequently interact with wet runback layers, thin freezing films, or partially solidified ice textures, all under strong aerodynamic shear. Evidence shows that runback rivulets and droplets are highly sensitive to airflow and surface wettability, producing oscillatory contact lines and modifying local thermal fields [174]. Oblique impacts on already wet or liquid-coated surfaces generate asymmetric crowns, splashing thresholds that vary with impact angle, and strong dependencies on film thickness and local tangential momentum [160]. When supercooled droplets strike freezing films, dendritic structures perturb crown formation and accelerate or suppress secondary-droplet generation depending on the surface state [170]. These coupled behaviors, combined with the fact that droplets in SLD environments strike after leading-edge passage at high inclination angles, point to the need for integrated studies resolving obliqueness, surface state (liquid/ice), and external airflow simultaneously, a combination that current literature only addresses little.

Together, these highlight that the absence of comprehensive datasets for high-speed, oblique SLD impacts on cold, wet, or ice-accreting surfaces under realistic aerodynamic loads remains a major bottleneck for advancing the predictive fidelity of runback ice models.

5. Coupled Surface Water Transport, Freezing, and Ice Accretion

5.1. Thermodynamic Effects and Non-Instantaneous Solidification

Most studies of droplet impact on dry surfaces or liquid films do not account for temperature variation, phase change, liquid subcooling, or thermal interaction with the underlying substrate [30,43,114,126,175,176]. The viscosity of supercooled water increases by at least threefold as the temperature drops from 20 °C to −15 °C. This physical change fundamentally alters the non-dimensional scaling that governs splashing. Specifically, while the Weber number remains relatively stable (as surface tension changes are minor), the Reynolds number decreases by a factor of three, and the Ohnesorge number increases by a factor of three. Theoretical models suggest this shift should stabilize the droplet. For instance, in the widely used Mundo correlation, the splashing parameter K scales with $\mu^{-0.25}$, implying that increased viscosity naturally lowers the propensity to splash. Experimental data confirm that increasing the liquid film temperature generally promotes the transition from spreading to splashing [177]. However, under real SLD icing conditions, these viscosity-driven trends interact with freezing, roughness evolution, and liquid redistribution, so the thermodynamic response cannot be inferred from hydrodynamic scaling alone.

Yang et al. [170] investigated the drop impact on a freezing film and compared their results to the standard room conditions. They found that dendritic ice, or tree-shaped crystallized ice, would be pushed out of the frozen film due to the impact of the SLDs. They reported that crown lifetime on a freezing film first increases and then decreases with film thickness, whereas under room-temperature conditions it increases monotonically with film thickness. The prematurely shortened crown lifetime could be attributed to the presence of dendritic ice crystals. The outcome of an SLD striking a freezing water film results in fewer secondary droplets compared to a room-temperature droplet impacting a room-temperature water film at the same thickness. These observations demonstrate that freezing fundamentally changes not only the final phase state but also the transient hydrodynamics of the impact itself.

Cui and Habashi [178] developed a dendritic freezing model for in-flight SLD impingement, capturing phase-change dynamics at subfreezing temperatures. The model simulates dendritic ice formation and growth within impacting SLDs, influencing ice morphology and adhesion. By incorporating non-equilibrium solidification kinetics, it improves predictions of ice microstructure that determine the mechanical properties of accreted ice, aiding understanding of the rime-to-glaze transition and runback water formation. Jia et al. [179] numerically and experimentally studied SLD icing on a rotating spinner, achieving good agreement between both approaches. They found that increasing effective tangential impact velocity increases droplet rebound and splashing, leading to higher droplet mass loss coefficient and reduced mass collection efficiency. They also observed that the icing thickness on the surface increases with the increase in the total impact velocity. These results show that, under realistic aerodynamic conditions, freezing, splashing, tangential impact, and final accretion thickness are tightly coupled.

5.2. Surface Water Runback, Rivulet/Bead Evolution, and Roughness Development

Once impact and partial freezing occur, the subsequent transport of unfrozen water as films, rivulets, or discrete beads becomes a governing process in SLD icing, since it redistributes liquid mass and determines where downstream freezing ultimately occurs. In practical icing environments, this process is not simply a passive consequence of impact; it actively alters the local substrate and feeds back into subsequent droplet interactions.

While much of the literature focuses on the static roughness of the substrate itself, in practical icing scenarios, the surface roughness is dynamic and self-generating. As illustrated in the work of Zhang et al. [141], the initial water film does not remain smooth, but it coalesces into rivulets and isolated water beads, driven by aerodynamic shear. These features act as protruding roughness elements for subsequent droplet impacts. This self-induced roughness alters the splashing threshold. Unlike a pristine surface, a surface covered in beads and rivulets presents a complex, non-uniform topography. When subsequent droplets impinge upon these sessile beads or rivulets, the effective impact angle changes locally, often resulting in off-normal collisions that lower the energy barrier for splashing. As noted in splashing studies, high roughness tends to trigger prompt splash significantly earlier than on smooth surfaces.

Furthermore, under freezing conditions, this roughness intensifies. Yang et al. [170] observed that dendritic ice crystals. These ice features disrupt the spreading lamella of incoming droplets, causing premature crown breakup and reducing the crown lifetime. Consequently, the growing ice surface creates a feedback loop: initial roughness (beads/rivulets) triggers early splashing, which redistributes water mass to form macroscopic roughness elements like feathers and horns, which in turn generate even more violent splashing and mass loss for future droplets.

5.3. Rime, Glaze, and Mixed Accretion Under SLD Conditions

The final ice morphology under SLD conditions is governed by the competition between local freezing and downstream liquid transport, which often produces glaze or mixed accretions rather than purely conformal rime-type deposits. In contrast to conventional cloud-sized droplets, which typically impinge close to the stagnation region and freeze rapidly after impact, SLDs possess much greater thermal mass and inertia. As a result, only a portion of the incoming water may freeze immediately upon impact, while the remaining liquid persists as unfrozen surface water and is transported downstream by aerodynamic shear [5,20]. This delayed-freezing behavior fundamentally alters the spatial distribution of water/ice on the airfoil surface and thereby changes the resulting ice morphology.

The relative tendency toward rime, glaze, or mixed accretion depends on the local freezing fraction, which is fundamentally controlled by the amount of water mass, surface and ambient temperature, convective/conductive heat transfer, and the residence time of the liquid before solidification. When the freezing fraction is high and most of the collected water solidifies locally, the resulting ice tends to be more compact and conformal. In contrast, when a significant fraction of the collected SLD mass remains liquid after impact, the water can spread, coalesce, and run back into colder downstream regions, where it freezes later as a more irregular and protruding accretion. Under such conditions, glaze-like or mixed ice is more likely to develop, especially when the local aerodynamic and thermal environment promotes persistent surface water transport rather than immediate solidification [11,22,24]

This distinction is especially important in SLD icing because the larger droplets not only extend the impingement limit farther aft but also enhance the formation of unfrozen runback water. The resulting surface water may initially form a continuous film and then transition into rivulets or isolated beads under the combined effects of aerodynamic shear, surface roughness, and local freezing [11]. Such redistribution of liquid mass strongly influences where freezing ultimately occurs, and therefore where hazardous protuberances or irregular ice structures emerge. Rather than producing a simple leading-edge accretion, SLD conditions often promote nonuniform downstream growth, which is one of the defining features distinguishing SLD icing from conventional small-droplet icing [7,20]

The morphology is further complicated by splashing and secondary-droplet re-impingement. As discussed in previous sections, high-inertia impacts may eject secondary droplets that are transported farther downstream and re-deposited in regions already influenced by runback water or partially frozen substrates. This process modifies the local water mass distribution, the instantaneous freezing fraction, and the roughness state of the surface, thereby introducing an additional feedback between impact dynamics and accretion morphology [7,11,12]. In this sense, rime-, glaze-, and mixed-type accretions under SLD conditions should not be viewed as purely thermodynamic states, but as outcomes of a strongly coupled transport process involving impact, splashing, liquid redistribution, and delayed phase change.

Recent studies on SLD microphysics and surface water evolution have further highlighted the importance of these coupled processes in determining downstream ice formation and surface roughness development [28–30,33]. These works collectively suggest that the key to understanding SLD accretion morphology is not merely whether a droplet freezes upon impact, but how much liquid remains mobile, how it interacts with the evolving air-water-ice interface, and where it ultimately solidifies under flight-relevant thermal and aerodynamic conditions.

5.4. Synthesis of Coupled SLD Ice-Accretion Physics

The studies reviewed in this section show that SLD ice accretion is governed by the coupling among droplet impact, surface water transport, heat transfer, and phase change. Non-instantaneous solidification allows a substantial portion of the impinged water to remain mobile, as freezing often lags behind the rapid hydrodynamic spreading and deformation of the droplet. Experiments and simulations show that during early impact on cold substrates, the bulk of the droplet can remain liquid because the time scale of heat transfer is slower than the fluid-dynamic deformation, leaving no macro-scale frozen layer in the initial stage [180]. Even after initial nucleation, a mixed liquid–solid region persists and the freezing front advances gradually, rather than instantaneously, enabling continued liquid motion along the surface [181]. Meanwhile, aerodynamic shear effectively redistributes this unfrozen water, driving it into films, rivulets, and bead-like structures prior to final freezing. Observations in icing-relevant shear flows confirm that runback water occurs as beads, continuous films, or rivulets, with transitions driven by airflow-induced interfacial fluctuations and shear stress [182]. Under high-speed aerodynamic forcing, water films can thin, rupture, and reorganize into rivulets or droplet-like structures, which then transport mass downstream before freezing [183].

Although individual elements of this process have been studied, including droplet-scale freezing dynamics, runback behavior under aerodynamic shear, and numerical treatments of multiphase interfacial evolution, a unified predictive framework remains incomplete, particularly under the combined influences of high-speed airflow, evolving surface roughness, and mixed rime–glaze accretion. Existing icing models and engineering tools acknowledge these limitations, noting that multi-physics coupling across droplet trajectories, phase change, and interfacial transport is still constrained by empirical assumptions and incomplete validation under realistic conditions [184]. Studies of SLD impingement on airfoils further emphasize that as ice accretes, surface roughness and geometry evolve dynamically, altering both local flow fields and subsequent droplet impact and runback patterns in ways current simulations struggle to capture [185]. Similarly, mixed rime–glaze regimes involve complex interactions between partial freezing, delayed solidification, and downstream refreezing, phenomena that remain difficult to predict accurately using existing Eulerian, Lagrangian, or SPH-based models [186,187]. This uncertainty is central to SLD icing prediction because the final ice shape depends not only on where droplets initially impinge, but also on where liquid water is transported and ultimately freezes downstream. Experimental and numerical evidence shows that runback water forms films, beads, and rivulets that are highly sensitive to aerodynamic shear, surface wettability, and evolving ice topology, leading to significant variations in downstream accretion locations [188]. Moreover, downstream runback ice has been shown to induce substantial aerodynamic penalties, including lift loss and earlier stall onset, highlighting the need for accurate prediction of water transport pathways and freezing locations [185]. These highlight that without a unified framework capable of capturing coupled aero-thermo-fluid processes over evolving surfaces, reliable prediction of SLD ice shapes, and thus aircraft performance degradation, remains challenging.

6. Impact on Ice Protection Technologies

While the Weber and Reynolds numbers provide a baseline for predicting splashing on idealized dry surfaces, they do not account for the physicochemical interaction between the fluid and the substrate. In practical aviation scenarios, the surface condition varies significantly, from untreated aluminum to advanced ice-phobic coatings. Consequently, the splashing threshold and post-impact morphology are heavily dictated by the surface wettability and texture. More importantly, the effectiveness of surface-based ice protection strategies under SLD conditions depends not only on their influence on impact and splash behavior but also on how they modify liquid retention, runback, freezing delay, and downstream accretion.

6.1. Drop Splashing on Hydrophilic Surfaces

Conventional aircraft surfaces without any treatment usually appear to be hydrophilic. When a droplet impacts such hydrophilic surfaces, the droplet could experience a sequence of dynamic stages, including initial contact, spreading, receding, splashing, and rebounding [37].

Figure 13 shows the time sequences of the dynamic droplet impinging process on a hydrophilic surface at the Weber number of ~3100 [32]. As the water droplet impinges on the hydrophilic surface, it is observed that the water mass would spread out in all directions to form a pancake-like structure over the hydrophilic surface with an intense splashing of the satellite water droplets at the boundary rim. As time goes by, the pancake-like structure keeps spreading until reaching its maximum contact area. After that, the pancake-like structure starts to recede with the water mass flowing from the spreading boundary back to the impinging center. During the spreading process, a thin water film with a much larger contact area (in comparison to the projected area of the water droplet) is formed over the hydrophilic surface. A large portion of the impinged water mass is kept on the hydrophilic surface during and after the impinging process. During an SLD icing event, such a hydrophilic surface would result in a rapid and tremendous ice accretion over the aircraft surfaces. The supercooled water mass can easily spread and adhere to the surface due to the rapid freezing process along with the impinging hydrodynamic process.

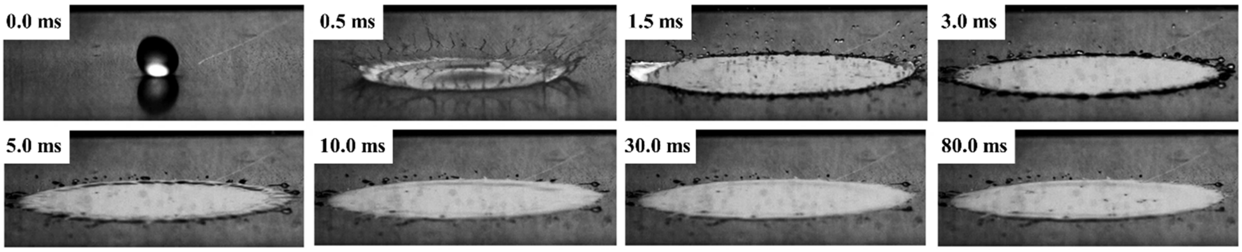

Figure 13. Time evolutions of the dynamic impinging process of water droplets onto a hydrophilic surface at the Weber number of $We \approx 3100$ [189].

6.2. Drop Splashing on Superhydrophobic Surfaces

In comparison to the hydrophilic surface, the droplet impinging process on a superhydrophobic surface appears to be very different, as shown in Figure 14 [32]. As the water droplet impinges onto the surface, the water mass is found to spread out rapidly to form an extremely thin water film over the superhydrophobic surface. Instead of forming a pancake-like water film, the spreading water mass is found to break into many tiny satellite droplets, which bounce off from the surface instantly. The water-repelling dynamics of this superhydrophobic surface are essentially due to the existence of the nano-/micro-scale roughness/textures on the surface. With the surface being kept at the Cassie–Baxter state, with air trapped in the surface texture beneath the droplet, the kinetic energy in the water droplet impact is not well dissipated during the spreading process but remains in the rebounded satellite droplets. As a result, only a small portion of the impinged water mass is left on the surface after the impinging process. The remaining water mass on the surface is also found to bead up with a very large contact angle and a considerably small contact area, which is considered to be a good indicator of reduced ice adhesion strength.

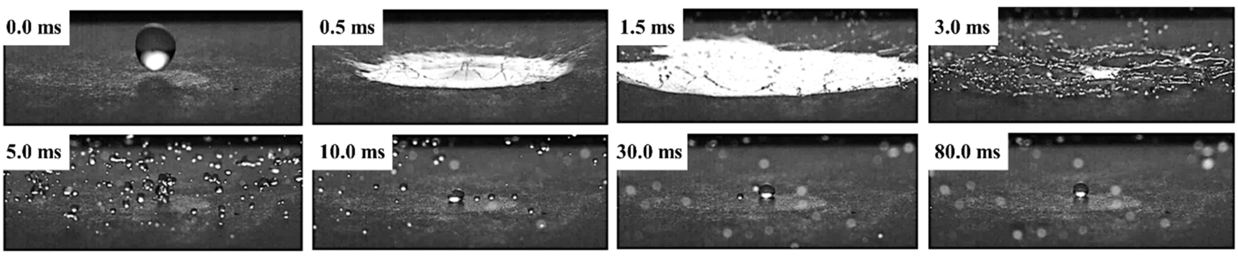

Figure 14. Time evolutions of the dynamic impinging process of water droplets onto a superhydrophobic surface at the Weber number of $We \approx 3100$ [189].

Shang et al. [190] showed that the temperature of the substrate plays a pivotal role in modulating these water-repelling dynamics, often defining the operational limits of superhydrophobic surfaces in cold environments (Figure 15). While the initial spreading

https://doi.org/10.3390/fluids11070162

phase remains largely temperature-independent, as it is dominated by inertial forces and occurs before significant heat transfer can alter the liquid's properties, the subsequent receding phase is highly sensitive to the surface temperature [190]. As the surface temperature decreases, the increasing viscosity of the liquid film enhances viscous dissipation, which progressively saps the kinetic energy required for a complete rebound. This results in a temperature-induced transition: at moderately cold temperatures, the droplet may still achieve a complete or partial rebound, but as the temperature drops further, the receding process is severely inhibited, leading to full adhesion and pinning. This behavior is fundamentally governed by the competition between the receding time of the liquid and the onset of freezing. If the receding process is not completed before the liquid–solid interface begins to freeze, the droplet remains trapped on the surface, forming distinct ice morphologies.

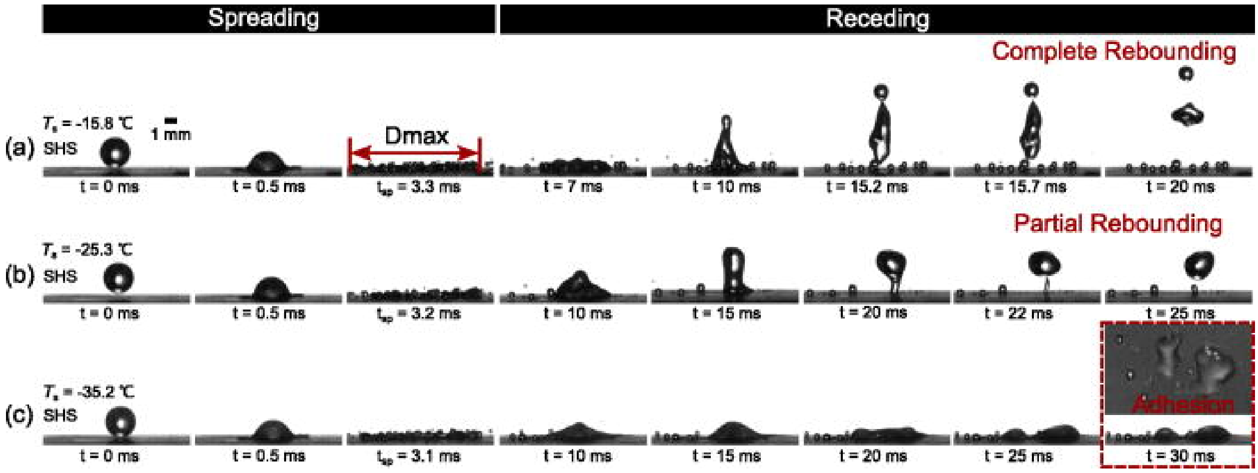

Figure 15. Dynamic behaviors of droplets on SHS at various wall surface temperatures [190].

6.3. Drop Splashing on Slippery Liquid-Infused Porous Surfaces (SLIPS)

Slippery liquid-infused porous surfaces represent another class of protective surfaces capable of inhibiting droplet splashing. By impregnating a porous or textured substrate with a lubricating liquid, these surfaces form a stable, smooth liquid interface that reduces contact-line pinning and enhances viscous dissipation during impact. As a result, lubricant-infused porous surfaces can effectively suppress droplet splashing and have received growing attention in recent years. SLIPSs, inspired by the Nepenthes pitcher plants, have the potential to be used as passive icephobic materials because they are able to reduce ice adhesion by 10 kPa, as measured by non-impact bulk ice [191,192].

Figure 16 shows the snapshot images to reveal the dynamic impinging process of a water droplet on an SLIPS at the Weber number of 4000 [193]. Upon the droplet impinging onto the SLIPS, similar spreading and splashing phenomena are observed at the early stage of the droplet impinging process. However, due to the hydrophobic nature of the SLIPS, the maximum spreading diameter of the water droplet on the SLIPS is found to be smaller than that over the hydrophilic surface, along with the formation of more splashing satellite droplets. During the receding process, while the contact area between the droplet and the surface becomes smaller, the inward-receding ring is found to break into more tiny water droplets. These satellite droplets are then found to coalesce and bounce off from the surface, leaving a very small amount of water mass on the SLIPS. Furthermore, unlike that of forming a large pancake-like water film on the hydrophilic surface, the remaining water mass on the SLIPS is found to break into many small droplets. Thus, the wetted area on the SLIPS becomes much smaller in comparison to that on the hydrophilic surface.

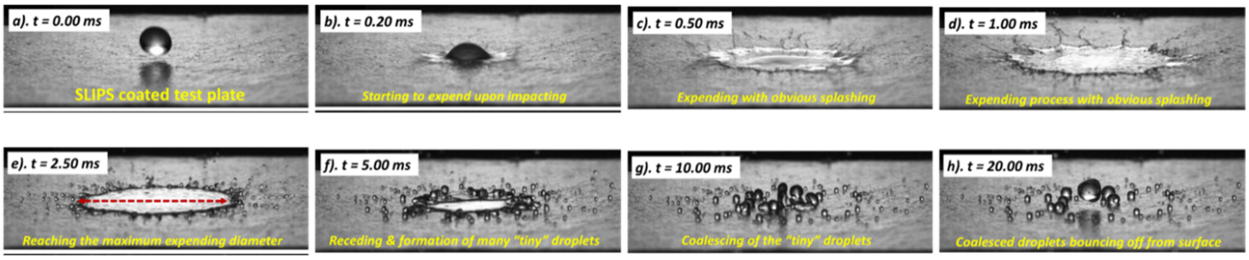

Figure 16. Time evolutions of the dynamic impinging process of a water droplet onto an SLIPS at the Weber number of $We \approx 4000$ [194].

Islam and Lian [195] investigated moderate- to high-speed impacts on slippery lubricated surfaces. They investigated bare surfaces with lubricant films and a porous microwell structure that holds the lubricant. With the lubricant films without any underlying structure they found that splashing phenomena are very different at different impact speeds. For speed impacts at 5 m/s, the water drop-lubricant travels laterally, but if the speed of impact is increased sixfold to 30 m/s, the water drop creates a secondary impingement and recirculatory disturbance, as shown in Figure 17.

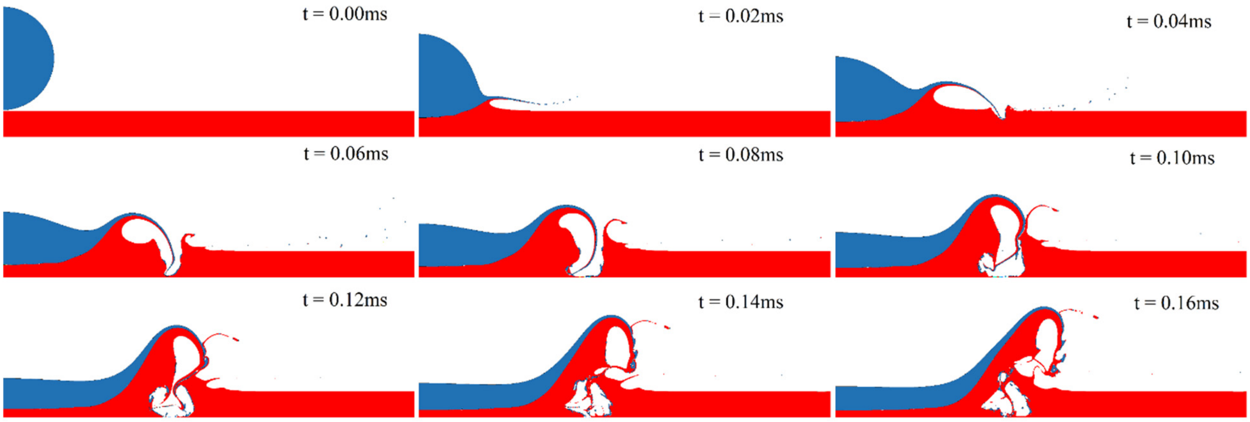

Figure 17. Drop impact on lubricant at 30 m/s, showing secondary impingement [195].

6.4. Drop Splashing on Soft PDMS Surface

Figure 18 shows the snapshot images to reveal the dynamic impinging process of a water droplet on a soft PDMS surface at the Weber number of 4000 [31]. Upon the impingement of the water droplet on the soft PDMS surface, the soft material is found to deform instantly due to suddenly increased impact stresses on the surface. Along with the deformation of the elastic PDMS material, the impinged water mass is found to be bounced off from the surface while it still undergoes the spreading-and-receding process. The dynamically deforming PDMS surface behaves like a trampoline, which bounces off the impinged water mass. The bounced water mass then breaks into many tiny satellite droplets, as shown in Figure 18. Thus, the wetted area on this surface can be substantially reduced, thereby mitigating the SLD icing on aircraft.

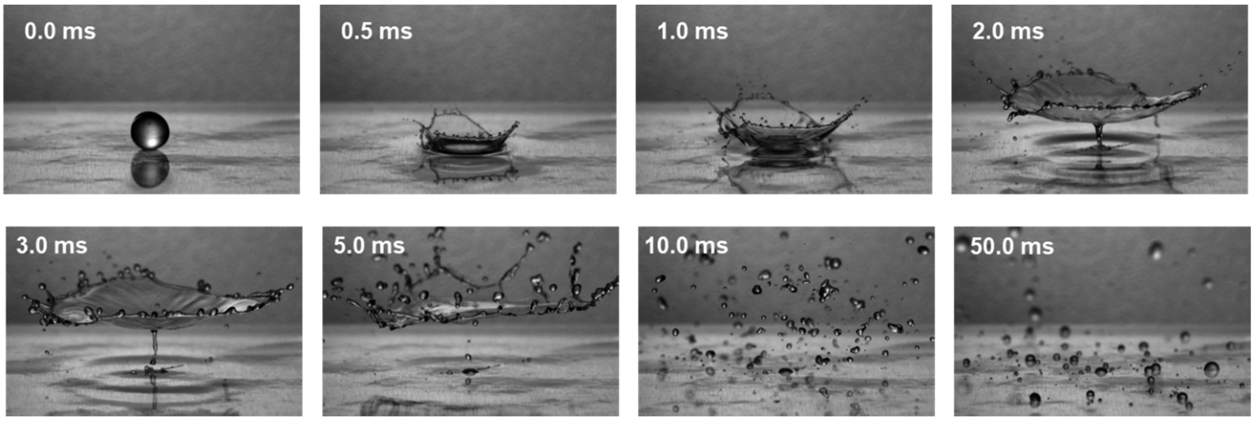

Figure 18. Time evolutions of the dynamic impinging process of a water droplet onto a soft PDMS surface at the Weber number of $We \approx 4000$ [194].

While superhydrophobic surfaces, liquid-infused porous surfaces, and compliant substrates have demonstrated significant potential for mitigating SLD impacts in controlled laboratory settings [128,196–198], their translation to practical aviation applications is currently impeded by severe durability and environmental stability concerns. A primary failure mode arises from thermodynamic conditions. Under high humidity, water condensation within the surface micro-textures can bridge the air pockets, leading to mechanical interlocking between the ice and the substrate that negates the surface's water-repellency [199,200]. Furthermore, the harsh operational envelope of flight imposes mechanical and chemical stresses rarely replicated in fundamental droplet impact studies. To maintain efficacy on a wing leading edge, these coatings must withstand high-speed rain erosion, prolonged UV radiation exposure, and intense aerodynamic shear forces without suffering texture degradation or lubricant depletion. Consequently, a significant disconnect remains between the initial aerodynamic benefits observed in the laboratory and the long-term structural integrity required for certification under realistic flight Reynolds numbers and weathering conditions.

6.5. Synthesis of Mitigation Strategies Under SLD Conditions

The reviewed surface-engineering approaches demonstrate that wettability, compliance, and lubricant infusion can modify droplet impact, reduce adhesion, delay freezing, or promote liquid and ice shedding. However, no single surface strategy fully addresses the coupled challenges of SLD icing, where high-speed impact, splashing, runback water, repeated droplet impingement, and delayed freezing occur simultaneously. Superhydrophobic and lubricant-infused surfaces are promising for reducing contact time and adhesion, but their durability, lubricant retention, erosion resistance, and performance under runback-water conditions remain uncertain. Therefore, future SLD mitigation strategies will likely require hybrid approaches that combine surface design with active anti-/de-icing systems and are validated under realistic aerodynamic and freezing conditions.

7. Conclusions

This review has summarized recent progress in understanding the microphysics of SLDs and their implications for aviation icing. Compared with conventional cloud-sized droplets, SLDs possess higher inertia, exhibit extended impingement limits, and are more likely to undergo splashing, secondary-droplet re-impingement, delayed freezing, and surface water runback. These coupled processes can promote ice accretion beyond protected leading-edge regions and remain difficult to predict using conventional icing models.

https://doi.org/10.3390/fluids11070162

Fundamental studies of droplet impact on dry and wet surfaces provide an essential basis for understanding SLD behavior. Classical regime classifications and splashing thresholds based on Reynolds, Weber, Ohnesorge, and K parameters have clarified the transition among deposition, rebound, prompt splashing, and corona splashing. However, most existing correlations were developed for low-speed, normal impacts under non-freezing conditions. Their direct application to aircraft SLD icing is therefore limited because practical encounters involve high-speed and often oblique impacts, external airflow, evolving wet or iced surfaces, and simultaneous heat transfer and phase change.

A key feature of SLD icing is the persistence and redistribution of unfrozen water after impact. Runback water may evolve from continuous films into rivulets and isolated beads before freezing into glaze, mixed, or irregular ice accretions. This interaction among splashing, liquid water transport, aerodynamic shear, heat transfer, freezing, and roughness evolution makes SLD ice accretion a highly coupled thermo-fluid problem and remains a major challenge for predictive modeling.

The reviewed literature also highlights important opportunities and limitations for icing mitigation. Surface-engineering approaches, including superhydrophobic, soft, and slippery liquid-infused porous surfaces, can modify impact outcomes, reduce adhesion, delay freezing, and promote liquid or ice shedding. However, their performance under realistic SLD conditions remains uncertain, particularly with respect to coating durability, erosion resistance, repeated high-speed impacts, runback-water stability, and unsteady ice accretion.

Overall, aircraft SLD icing should be viewed not simply as a droplet-impact problem, but as a coupled process involving high-speed impingement, splashing, secondary-droplet generation, delayed solidification, runback, and downstream ice growth. This paper mainly focuses on the dynamics of droplet impact and splashing, while the effects of impact behavior on nucleation, heat transfer and ice crystal growth remain to be further investigated. Future progress will require integrated experimental, theoretical, and computational studies under aircraft-relevant conditions. Such efforts are essential for improving SLD icing prediction and for developing robust, application-ready anti-/de-icing strategies.

Author Contributions: Y.L. (Yongsheng Lian) and H.H. conceptualized the paper. Y.G., Y.L. (Yang Liu), M.S., H.H. and Y.L. (Yongsheng Lian) all prepared the draft. All authors have read and agreed to the published version of the manuscript.

Funding: This research received no external funding.

Informed Consent Statement: Not applicable.

Institutional Review Board Statement: Not applicable.

Data Availability Statement: The raw data supporting the conclusions of this article will be made available by the authors on request.

Conflicts of Interest: The authors declare no conflict of interest.

References

1. Landsberg, B. *AOPA Safety Advisor: Aircraft Icing*; AOPA Air Safety Foundation: Frederick, MD, USA, 2008; p. 2.
2. Bragg, M.; Gregorek, G.; Lee, J. Airfoil aerodynamics in icing conditions. *J. Aircr.* **1986**, *23*, 76–81.
3. Poots, G.; Gent, R.W.; Dart, N.P.; Cansdale, J.T. Aircraft icing. Philosophical Transactions of the Royal Society of London. *Ser. A Math. Phys. Eng. Sci.* **2000**, *358*, 2873–2911. https://doi.org/10.1098/rsta.2000.0689.
4. Bragg, M.B.; Broeren, A.P.; Blumenthal, L.A. Iced-airfoil aerodynamics. *Prog. Aerosp. Sci.* **2005**, *41*, 323–362.
5. Politovich, M.K. Aircraft icing caused by large supercooled droplets. *J. Appl. Meteorol. Climatol.* **1989**, *28*, 856–868.

6. Bidwell, C. Icing calculations for a 3D, high-lift wing configuration. In Proceedings of the 43rd AIAA Aerospace Sciences Meeting and Exhibit, Reno, NV, USA, 10–13 January 2005.
7. Wright, W.; Potapczuk, M. Semi-empirical modelling of SLD physics. In Proceedings of the 42nd AIAA Aerospace Sciences Meeting and Exhibit, Reno, NV, USA, 5–8 January 2004.
8. Rutkowski, A.; Wright, W.; Potapczuk, M. Numerical study of droplet splashing and re-impingement. In Proceedings of the 41st Aerospace Sciences Meeting and Exhibit, Reno, NV, USA, 6–9 January 2003.
9. Burzynski, D.A.; Roisman, I.V.; Bansmer, S.E. On the splashing of high-speed drops impacting a dry surface. *J. Fluid Mech.* **2020**, *892*, A2.
10. Cebeci, T.; Kafyeke, F. Aircraft icing. *Annu. Rev. Fluid Mech.* **2003**, *35*, 11–21.
11. Anderson, D.N.; Tsao, J.-C. *Ice Shape Scaling for Aircraft in SLD Conditions*; Amazon: Seattle, DC, USA, 2008.
12. Bond, T.; Potapczuk, M.; Miller, D. Overview of SLD engineering tool development. In Proceedings of the 41st Aerospace Sciences Meeting and Exhibit, Reno, NV, USA, 6–9 January 2003.
13. Stow, C.D.; Hadfield, M.G. An experimental investigation of fluid flow resulting from the impact of a water drop with an unyielding dry surface. *Proc. R. Soc. Lond. A Math. Phys. Sci.* **1981**, *373*, 419–441.
14. Mundo, C.; Sommerfeld, M.; Tropea, C. Droplet-wall collisions: Experimental studies of the deformation and breakup process. *Int. J. Multiph. Flow* **1995**, *21*, 151–173.
15. Jung, S.; Myong, R. Numerical modeling for eulerian droplet impingement in supercooled large droplet conditions. In Proceedings of the 51st AIAA Aerospace Sciences Meeting including the New Horizons Forum and Aerospace Exposition, Grapevine, TX, USA, 7–10 January 2013.
16. Xu, L.; Zhang, W.W.; Nagel, S.R. Drop splashing on a dry smooth surface. *Phys. Rev. Lett.* **2005**, *94*, 184505.
17. Xu, L.; Barcos, L.; Nagel, S.R. Splashing of liquids: Interplay of surface roughness with surrounding gas. *Phys. Rev. E* **2007**, *76*, 066311.
18. Latka, A.; Strandburg-Peshkin, A.; Driscoll, M.M.; Stevens, C.S.; Nagel, S.R. Creation of prompt and thin-sheet splashing by varying surface roughness or increasing air pressure. *Phys. Rev. Lett.* **2012**, *109*, 054501.
19. Potapczuk, M.; Al-khalil, K.; Velazquez, M. Ice accretion and performance degradation calculations with LEWICE/NS. In Proceedings of the 31st Aerospace Sciences Meeting, Reno, NV, USA, 11–14 January 1993.
20. Bragg, M. Aerodynamics of supercooled-large-droplet ice accretions and the effect on aircraft control. In Proceedings of the FAA International Conference on Aircraft Inflight Icing, Springfield, VA, USA, 6–8 May 1996.
21. Waldman, R.; Liu, Y.; Zhang, K.; Hu, H. High-speed imaging to quantify the transient ice accretion process on a NACA 0012 airfoil. In Proceedings of the 53rd AIAA Aerospace Sciences Meeting, Kissimmee, FL, USA, 5–9 January 2015.
22. Thompson, B.E.; Marrochello, M.R. Rivulet formation in surface-water flow on an airfoil in rain. *AIAA J.* **1999**, *37*, 45–49.
23. Hansman, R.J., Jr.; Turnock, S.R. Investigation of surface water behavior during glaze ice accretion. *J. Aircr.* **1989**, *26*, 140–147.
24. Wan, T.; Wu, S.-W. Aerodynamic analysis under influence of heavy rain. *J. Aeronaut. Astronaut. Aviat.* **2004**, *41*, 173–180.
25. Wright, W.B.; Potapczuk, M.G. *Computational Simulation of Large Droplet Icing*; National Aeronautics and Space Administration: Washington, DC, USA, 1996.
26. Li, H.; Roisman, I.V.; Tropea, C. Influence of solidification on the impact of supercooled water drops onto cold surfaces. *Exp. Fluids* **2015**, *56*, 133.
27. Work, A.; Lian, Y. A critical review of the measurement of ice adhesion to solid substrates. *Prog. Aerosp. Sci.* 2018, **98**, 1–26.
28. Cao, Y.; Wu, Z.; Xu, Z. Effects of rainfall on aircraft aerodynamics. *Prog. Aerosp. Sci.* **2014**, *71*, 85–127.
29. Zhang, K.; Wei, T.; Hu, H. An experimental investigation on the surface water transport process over an airfoil by using a digital image projection technique. *Exp. Fluids* **2015**, *56*, 173.
30. Liu, Y.; Chen, W.-L.; Bond, L.; Hu, H. An experimental study on the characteristics of wind-driven surface water film flows by using a multi-transducer ultrasonic pulse-echo technique. *Phys. Fluids* **2017**, *29*, 012102. https://doi.org/10.1063/1.4973398.
31. Liu, Y.; Ma, L.; Wang, W.; Kota, A.K.; Hu, H. An experimental study on soft PDMS materials for aircraft icing mitigation. *Appl. Surf. Sci.* **2018**, *447*, 599–609.
32. Liu, Y.; Li, L.; Li, H.; Hu, H. An experimental study of surface wettability effects on dynamic ice accretion process over an UAS propeller model. *Aerosp. Sci. Technol.* **2018**, *73*, 164–172.
33. Liu, Y.; Hu, H. An experimental investigation on the unsteady heat transfer process over an ice accreting airfoil surface. *Int. J. Heat Mass Transf.* **2018**, *122*, 707–718. https://doi.org/10.1016/j.ijheatmasstransfer.2018.02.023.
34. Alary, T.; Déjean, B.; Berthoumieu, P.; Trontin, P. Supercooled large droplet (SLD) impact on ice at high velocity: Splashing characterization. In Proceedings of the AIAA Aviation 2022 Forum, Chicago, IL, USA, 27 June–1 July 2022.

35. Dejean, B.; Alary, T.; Duchayne, Q.; Berthoumieu, P. Influence of Realistic Aircraft Conditions on Accretion of Supercooled Large Droplet. In Proceedings of the International Conference on Icing of Aircraft, Engines, and Structures, Vienna, Austria, 20–22 June 2023.
36. Berthoumieu, P.; Déjean, B.; Bodoc, V.; Alary, T. ONERA research icing wind tunnel. In Proceedings of the AIAA Aviation 2022 Forum, Chicago, IL, USA, 27 June–1 July, 2022.
37. Rioboo, R.; Tropea, C.; Marengo, M. Outcomes from a drop impact on solid surfaces. *At. Sprays* **2001**, *11*, 155–166.
38. Liu, Y.; Yan, X.; Wang, Z. Droplet dynamics on slippery surfaces: Small droplet, big impact. *Biosurface Biotribol.* **2019**, *5*, 35–45.
39. Bartolo, D.; Josserand, C.; Bonn, D. Singular jets and bubbles in drop impact. *Phys. Rev. Lett.* **2006**, *96*, 124501.
40. Tsai, P.; Hendrix, M.H.; Dijkstra, R.R.; Shui, L.; Lohse, D. Microscopic structure influencing macroscopic splash at high Weber number. *Soft Matter* **2011**, *7*, 11325–11333.
41. Chandra, S.; Avedisian, C. On the collision of a droplet with a solid surface. *Proc. R. Soc. Lond. Ser. A Math. Phys. Sci.* **1991**, *432*, 13–41.
42. Xu, H.; Liu, Y.; He, P.; Wang, H. The TAR model for calculation of droplet/wall impingement. *J. Fluids Eng.* **1998**, *120*, 593–597.
43. Roisman, I.V.; Tropea, C. Impact of a drop onto a wetted wall: Description of crown formation and propagation. *J. Fluid Mech.* **2002**, *472*, 373–397.
44. Kim, H.-Y.; Chun, J.-H. The recoiling of liquid droplets upon collision with solid surfaces. *Phys. Fluids* **2001**, *13*, 643–659.
45. Brant Foote, G. A numerical method for studying liquid drop behavior: Simple oscillation. *J. Comput. Phys.* **1973**, *11*, 507–530. https://doi.org/10.1016/0021-9991(73)90135-6.
46. Pasandideh-Fard, M.; Aziz, S.; Chandra, S.; Mostaghimi, J. Cooling effectiveness of a water drop impinging on a hot surface. *Int. J. Heat Fluid Flow* **2001**, *22*, 201–210.
47. Bussmann, M.; Mostaghimi, J.; Chandra, S. On a three-dimensional volume tracking model of droplet impact. *Phys. Fluids* **1999**, *11*, 1406–1417.
48. Aksoy, Y.T.; Eneren, P.; Koos, E.; Vetrano, M.R. Spreading of a droplet impacting on a smooth flat surface: How liquid viscosity influences the maximum spreading time and spreading ratio. *Phys. Fluids* **2022**, *34*, 042106.
49. Mundo, C.; Sommerfeld, M.; Tropea, C. On the modeling of liquid sprays impinging on surfaces. *At. Sprays* **1998**, *8*, 625–652.
50. Xu, L. Liquid drop splashing on smooth, rough, and textured surfaces. *Phys. Rev. E* **2007**, *75*, 056316.
51. Mandre, S.; Brenner, M.P. The mechanism of a splash on a dry solid surface. *J. Fluid Mech.* **2012**, *690*, 148–172.
52. Schmehl, R.; Rosskamp, H.; Willmann, M.; Wittig, S. CFD analysis of spray propagation and evaporation including wall film formation and spray/film interactions. *Int. J. Heat Fluid Flow* **1999**, *20*, 520–529.
53. Wal, R.L.V.; Berger, G.M.; Mozes, S.D. The splash/non-splash boundary upon a dry surface and thin fluid film. *Exp. Fluids* **2006**, *40*, 53–59.
54. Palacios, J.; Hernández, J.; Gómez, P.; Zanzi, C.; López, J. Experimental study of splashing patterns and the splashing/deposition threshold in drop impacts onto dry smooth solid surfaces. *Exp. Therm. Fluid Sci.* **2013**, *44*, 571–582. https://doi.org/10.1016/j.expthermflusci.2012.08.020.
55. Walzel, P. Zerteilgrenze beim Tropfenprall. *Chem. Ing. Tech.* **1980**, *52*, 338–339. https://doi.org/10.1002/cite.330520412.
56. Schmidt, P.; Knauss, G. Prallzerstäubung von Flüssigkeiten bei Nichtbenetzung. *Chem. Ing. Tech.* **1976**, *48*, 659. https://doi.org/10.1002/cite.330480724.
57. Hardalupas, Y.; Taylor, A.M.K.P.; Wilkins, J.H. Experimental investigation of sub-millimetre droplet impingement on to spherical surfaces. *Int. J. Heat Fluid Flow* **1999**, *20*, 477–485. https://doi.org/10.1016/S0142-727X(99)00045-4.
58. Cossali, G.E.; Coghe, A.; Marengo, M. The impact of a single drop on a wetted solid surface. *Exp. Fluids* **1997**, *22*, 463–472.
59. Range, K.; Feuillebois, F. Influence of surface roughness on liquid drop impact. *J. Colloid Interface Sci.* **1998**, *203*, 16–30.
60. Vander Wal, R.L.; Berger, G.M.; Mozes, S.D. The combined influence of a rough surface and thin fluid film upon the splashing threshold and splash dynamics of a droplet impacting onto them. *Exp. Fluids* **2006**, *40*, 23–32.
61. Riboux, G.; Gordillo, J.M. Experiments of drops impacting a smooth solid surface: A model of the critical impact speed for drop splashing. *Phys. Rev. Lett.* **2014**, *113*, 024507.
62. Roisman, I.V.; Lembach, A.; Tropea, C. Drop splashing induced by target roughness and porosity: The size plays no role. *Adv. Colloid Interface Sci.* **2015**, *222*, 615–621.
63. Bird, J.C.; Tsai, S.S.; Stone, H.A. Inclined to splash: Triggering and inhibiting a splash with tangential velocity. *New J. Phys.* **2009**, *11*, 063017.
64. Hao, J. Effect of surface roughness on droplet splashing. *Phys. Fluids* **2017**, *29*, 122105.

65. De Goede, T.; Laan, N.; De Bruin, K.; Bonn, D. Effect of wetting on drop splashing of Newtonian fluids and blood. *Langmuir* **2017**, *34*, 5163–5168.
66. Almohammadi, H.; Amirfazli, A. Droplet impact: Viscosity and wettability effects on splashing. *J. Colloid Interface Sci.* **2019**, *553*, 22–30. https://doi.org/10.1016/j.jcis.2019.05.101.
67. Quetzeri-Santiago, M.A.; Castrejón-Pita, A.A.; Castrejón-Pita, J.R. The effect of surface roughness on the contact line and splashing dynamics of impacting droplets. *Sci. Rep.* **2019**, *9*, 15030.
68. Ashida, T.; Watanabe, M.; Kobayashi, K.; Fujii, H.; Sanada, T. Hidden prompt splashing by corona splashing at drop impact on a smooth dry surface. *Phys. Rev. Fluids* **2020**, *5*, 011601. https://doi.org/10.1103/PhysRevFluids.5.011601.
69. Zhang, H.; Zhang, X.; Yi, X.; He, F.; Niu, F.; Hao, P. Reversed role of liquid viscosity on drop splash. *Phys. Fluids* **2021**, *33*, 052103.
70. García-Geijo, P.; Quintero, E.; Riboux, G.; Gordillo, J. Spreading and splashing of drops impacting rough substrates. *J. Fluid Mech.* **2021**, *917*, A50.
71. Yang, L.; Li, Z.; Yang, T.; Chi, Y.; Zhang, P. Experimental study on droplet splash and receding breakup on a smooth surface at atmospheric pressure. *Langmuir* **2021**, *37*, 10838–10848.
72. Aksoy, Y.T.; Eneren, P.; Koos, E.; Vetrano, M.R. Spreading-splashing transition of nanofluid droplets on a smooth flat surface. *J. Colloid Interface Sci.* **2022**, *606*, 434–443.
73. Liu, Y.; Gou, Y.; Lei, J.; Li, J.; Shen, S. Splashing characteristics and dynamics of drops impingement on ultracold surfaces. *Exp. Therm. Fluid Sci.* **2023**, *144*, 110863.
74. Tian, B.; Li, F.; Xiao, F.; Li, P.; Yang, X.; Liu, Y.; Xue, Y. Numerical investigation of splash modes and mechanisms for tiny droplet oblique impact on a dry smooth surface. *Phys. Fluids* **2025**, *37*, 092103.
75. Yang, S.; Pogu, P.-A.; Hou, Y.; Xia, K.; Reddyhoff, T.; Yu, M. From spreading to splashing: Interfacial phenomena of an ethanol droplet impacts on ultracold surfaces. *Surf. Interfaces* **2025**, *73*, 107620.
76. Foltyn, P.; Ribeiro, D.; Silva, A.; Lamanna, G.; Weigand, B. Influence of wetting behavior on the morphology of droplet impacts onto dry-patterned micro-structured surfaces. *Phys. Fluids* **2022**, *34*, 123322.
77. Vander Wal, R.L.; Berger, G.M.; Mozes, S.D. Droplets splashing upon films of the same fluid of various depths. *Exp. Fluids* **2006**, *40*, 33–52.
78. Che, Z.; Matar, O.K. Impact of droplets on immiscible liquid films. *Soft Matter* **2018**, *14*, 1540–1551.
79. Séon, T.; Ghabache, E.; Josserand, C. Frozen Impacted Drop: From Fragmentation to Hierarchical Crack Patterns. In Proceedings of the APS Division of Fluid Dynamics Meeting Abstracts, Portland, OR, USA, 20–22 November 2016.
80. Gordillo, L.; Sun, T.-P.; Cheng, X. Dynamics of drop impact on solid surfaces: Evolution of impact force and self-similar spreading. *J. Fluid Mech.* **2018**, *840*, 190–214.
81. Haller, K.; Poulikakos, D.; Ventikos, Y.; Monkewitz, P. Shock wave formation in droplet impact on a rigid surface: Lateral liquid motion and multiple wave structure in the contact line region. *J. Fluid Mech.* **2003**, *490*, 1–14.
82. Guo, Y.; Lian, Y.; Sussman, M. Investigation of drop impact on dry and wet surfaces with consideration of surrounding air. *Phys. Fluids* **2016**, *28*, 073303.
83. Jayaratne, O.; Mason, B.J. The coalescence and bouncing of water drops at an air/water interface. *Proc. R. Soc. Lond. Ser. A Math. Phys. Sci.* **1964**, *280*, 545–565.
84. Šikalo, Š.; Wilhelm, H.-D.; Roisman, I.; Jakirlić, S.; Tropea, C. Dynamic contact angle of spreading droplets: Experiments and simulations. *Phys. Fluids* **2005**, *17*, 062103.
85. Fukai, J.; Shiiba, Y.; Yamamoto, T.; Miyatake, O.; Poulikakos, D.; Megaridis, C.M.; Zhao, Z. Wetting effects on the spreading of a liquid droplet colliding with a flat surface: Experiment and modeling. *Phys. Fluids* **1995**, *7*, 236–247.
86. Zhao, H.-K.; Merriman, B.; Osher, S.; Wang, L. Capturing the behavior of bubbles and drops using the variational level set approach. *J. Comput. Phys.* **1998**, *143*, 495–518.
87. Weiss, D.A.; Yarin, A.L. Single drop impact onto liquid films: Neck distortion, jetting, tiny bubble entrainment, and crown formation. *J. Fluid Mech.* **1999**, *385*, 229–254.
88. Bussmann, M.; Chandra, S.; Mostaghimi, J. Modeling the splash of a droplet impacting a solid surface. *Phys. Fluids* **2000**, *12*, 3121–3132.
89. Zheng, L.; Zhang, H. An adaptive level set method for moving-boundary problems: Application to droplet spreading and solidification. *Numer. Heat Transf. Part B Fundam.* **2000**, *37*, 437–454.
90. Tanguy, S.; Berlemont, A. Application of a level set method for simulation of droplet collisions. *Int. J. Multiph. Flow* **2005**, *31*, 1015–1035.

91. Sussman, M.; Almgren, A.S.; Bell, J.B.; Colella, P.; Howell, L.H.; Welcome, M.L. An adaptive level set approach for incompressible two-phase flows. *J. Comput. Phys.* **1999**, *148*, 81–124.
92. Lesser, M.; Field, J. The impact of compressible liquids. *Annu. Rev. Fluid Mech.* **1983**, *15*, 97–122.
93. Mani, M.; Mandre, S.; Brenner, M.P. Events before droplet splashing on a solid surface. *J. Fluid Mech.* **2010**, *647*, 163–185.
94. Thoroddsen, S.T.; Takehara, K.; Etoh, T. Micro-splashing by drop impacts. *J. Fluid Mech.* **2012**, *706*, 560–570.
95. Yarin, A.L.; Weiss, D.A. Impact of drops on solid surfaces: Self-similar capillary waves, and splashing as a new type of kinematic discontinuity. *J. Fluid Mech.* **1995**, *283*, 141–173.
96. Yarin, A.L. Drop impact dynamics: Splashing, spreading, receding, bouncing. *Annu. Rev. Fluid Mech.* **2006**, *38*, 159–192.
97. Driscoll, M.M.; Nagel, S.R. Ultrafast interference imaging of air in splashing dynamics. *Phys. Rev. Lett.* **2011**, *107*, 154502.
98. Liu, Y.; Tan, P.; Xu, L. Kelvin–Helmholtz instability in an ultrathin air film causes drop splashing on smooth surfaces. *Proc. Natl. Acad. Sci. USA* **2015**, *112*, 3280–3284.
99. Agbaglah, G.; Deegan, R. Growth and instability of the liquid rim in the crown splash regime. *J. Fluid Mech.* **2014**, *752*, 485–496.
100. Allen, R.F. The role of surface tension in splashing. *J. Colloid Interface Sci.* **1975**, *51*, 350–351.
101. Mehdizadeh, N.Z.; Chandra, S.; Mostaghimi, J. Formation of fingers around the edges of a drop hitting a metal plate with high velocity. *J. Fluid Mech.* **2004**, *510*, 353–373.
102. Thoroddsen, S.; Sakakibara, J. Evolution of the fingering pattern of an impacting drop. *Phys. Fluids* **1998**, *10*, 1359–1374.
103. Bhola, R.; Chandra, S. Parameters controlling solidification of molten wax droplets falling on a solid surface. *J. Mater. Sci.* **1999**, *34*, 4883–4894.
104. Ahumada Lazo, J.; Liu, Y. Droplet impact on plasma surfaces: An interplay of the four states of matter. *Nat. Commun.* **2025**, *16*, 10018.
105. Burzynski, D.A.; Bansmer, S.E. Role of surrounding gas in the outcome of droplet splashing. *Phys. Rev. Fluids* **2019**, *4*, 073601. https://doi.org/10.1103/PhysRevFluids.4.073601.
106. Lian, Y. Numerical simulation of supercooled large droplets using the moment of fluid method. In Proceedings of the 52nd Aerospace Sciences Meeting, Harbor, MD, USA, 13–17 January 2014.
107. Rein, M. Phenomena of liquid drop impact on solid and liquid surfaces. *Fluid Dyn. Res.* **1993**, *12*, 61–93.
108. Motzkus, C.; Gensdarmes, F.; Géhin, E. Parameter study of microdroplet formation by impact of millimetre-size droplets onto a liquid film. *J. Aerosol Sci.* **2009**, *40*, 680–692.
109. Guo, Y.; Lian, Y. High-speed oblique drop impact on thin liquid films. *Phys. Fluids* **2017**, *29*, 082108.
110. Josserand, C.; Zaleski, S. Droplet splashing on a thin liquid film. *Phys. Fluids* **2003**, *15*, 1650–1657.
111. Deegan, R.; Brunet, P.; Eggers, J. Complexities of splashing. *Nonlinearity* **2007**, *21*, C1.
112. Ribeiro, D.F.; Silva, A.R.; Panão, M.R. Insights into Single Droplet Impact Models upon Liquid Films Using Alternative Fuels for Aero-Engines. *Appl. Sci.* **2020**, *10*, 6698.
113. Brackbill, J.U.; Kothe, D.B.; Zemach, C. A continuum method for modeling surface tension. *J. Comput. Phys.* **1992**, *100*, 335–354.
114. Zhu, J.; Tu, C.; Lu, T.; Luo, Y.; Zhang, K.; Chen, X. Behavior of a water droplet impacting a thin water film. *Exp. Fluids* **2021**, *62*, 143. https://doi.org/10.1007/s00348-021-03245-0.
115. Rieber, M.; Frohn, A. A numerical study on the mechanism of splashing. *Int. J. Heat Fluid Flow* **1999**, *20*, 455–461. https://doi.org/10.1016/S0142-727X(99)00033-8.
116. Gueyffier, D.; Zaleski, S. Formation de digitations lors de l'impact d'une goutte sur un film liquide. *Comptes Rendus L'académie Sci.-Ser. IIB-Mech.-Phys.-Astron.* **1998**, *326*, 839–844.
117. Trujillo, M.; Lee, C. Modeling crown formation due to the splashing of a droplet. *Phys. Fluids* **2001**, *13*, 2503–2516.
118. Thoroddsen, S.T. The ejecta sheet generated by the impact of a drop. *J. Fluid Mech.* **2002**, *451*, 373–381. https://doi.org/10.1017/S0022112001007030.
119. Thoroddsen, S.T.; Thoraval, M.-J.; Takehara, K.; Etoh, T. Droplet splashing by a slingshot mechanism. *Phys. Rev. Lett.* **2011**, *106*, 034501.
120. Nikolopoulos, N.; Theodorakakos, A.; Bergeles, G. Three-dimensional numerical investigation of a droplet impinging normally onto a wall film. *J. Comput. Phys.* **2007**, *225*, 322–341.
121. Fullana, J.M.; Zaleski, S. Stability of a growing end rim in a liquid sheet of uniform thickness. *Phys. Fluids* **1999**, *11*, 952–954. https://doi.org/10.1063/1.869989.
122. Roisman, I.V.; Horvat, K.; Tropea, C. Spray impact: Rim transverse instability initiating fingering and splash, and description of a secondary spray. *Phys. Fluids* **2006**, *18*, 102104. https://doi.org/10.1063/1.2364187.

123. Krechetnikov, R.; Homsy, G.M. Crown-forming instability phenomena in the drop splash problem. *J. Colloid Interface Sci.* **2009**, *331*, 555–559.
124. Rao, S.J.; Basu, S. Secondary Atomization of Droplets at Extreme Conditions. *Annu. Rev. Fluid Mech.* **2026**, *58*, 83–110. https://doi.org/10.1146/annurev-fluid-112823-115348.
125. Gao, X.; Li, R. Impact of a single drop on a flowing liquid film. *Phys. Rev. E* **2015**, *92*, 053005.
126. Rioboo, R.; Bauthier, C.; Conti, J.; Voue, M.; De Coninck, J. Experimental investigation of splash and crown formation during single drop impact on wetted surfaces. *Exp. Fluids* **2003**, *35*, 648–652.
127. Chen, N.; Chen, H.; Amirfazli, A. Drop impact onto a thin film: Miscibility effect. *Phys. Fluids* **2017**, *29*, 092106.
128. Ali, H.M.; Qasim, M.A.; Malik, S.; Murtaza, G. Techniques for the fabrication of super-hydrophobic surfaces and their heat transfer applications. *Heat Transf. Models Methods Appl.* **2018**, *1*, 283–315.
129. Kittel, H.M.; Roisman, I.V.; Tropea, C. Splash of a drop impacting onto a solid substrate wetted by a thin film of another liquid. *Phys. Rev. Fluids* **2018**, *3*, 073601.
130. Wang, A.-B.; Chen, C.-C. Splashing impact of a single drop onto very thin liquid films. *Phys. Fluids* **2000**, *12*, 2155–2158.
131. Geppert, A.; Chatzianagnostou, D.; Meister, C.; Gomaa, H.; Lamanna, G.; Weigand, B. Classification of impact morphology and splashing/deposition limit for n-hexadecane. *At. Sprays* **2016**, *26*, 983–1007. https://doi.org/10.1615/AtomizSpr.2015013352.
132. Geppert, A.; Terzis, A.; Lamanna, G.; Marengo, M.; Weigand, B. A benchmark study for the crown-type splashing dynamics of one-and two-component droplet wall–film interactions. *Exp. Fluids* **2017**, *58*, 172.
133. Bernard, R.; Baumgartner, D.; Brenn, G.; Planchette, C.; Weigand, B.; Lamanna, G. Miscibility and wettability: How interfacial tension influences droplet impact onto thin wall films. *J. Fluid Mech.* **2021**, *908*, A36.
134. Samenfink, W.; Elsäßer, A.; Dullenkopf, K.; Wittig, S. Droplet interaction with shear-driven liquid films: Analysis of deposition and secondary droplet characteristics. *Int. J. Heat Fluid Flow* **1999**, *20*, 462–469.
135. Hao, J.; Green, S.I. Splash threshold of a droplet impacting a moving substrate. *Phys. Fluids* **2017**, *29*, 012103. https://doi.org/10.1063/1.4972976.
136. Nikolopoulos, N.; Theodorakakos, A.; Bergeles, G. Normal impingement of a droplet onto a wall film: A numerical investigation. *Int. J. Heat Fluid Flow* **2005**, *26*, 119–132.
137. Castillo-Orozco, E.; Davanlou, A.; Choudhury, P.K.; Kumar, R. Droplet impact on deep liquid pools: Rayleigh jet to formation of secondary droplets. *Phys. Rev. E* **2015**, *92*, 053022.
138. Zhang, L.V.; Brunet, P.; Eggers, J.; Deegan, R.D. Wavelength selection in the crown splash. *Phys. Fluids* **2010**, *22*, 122105.
139. Honsek, R.; Habashi, W.G.; Aubé, M.S. Eulerian modeling of in-flight icing due to supercooled large droplets. *J. Aircr.* **2008**, *45*, 1290–1296.
140. Shetabivash, H.; Ommi, F.; Heidarinejad, G. Numerical analysis of droplet impact onto liquid film. *Phys. Fluids* **2014**, *26*, 012102.
141. Zhang, K.; Hu, H. An Experimental Study of the Wind-Driven Water Droplet/Rivulet Flows Over an Airfoil Pertinent to Wind Turbine Icing Phenomena. In Proceedings of the ASME 2014 4th Joint US-European Fluids Engineering Division Summer Meeting collocated with the ASME 2014 12th International Conference on Nanochannels, Microchannels, and Minichannels, Chicago, IL, USA, 3–7 August 2014.
142. Mukherjee, S.; Abraham, J. Crown behavior in drop impact on wet walls. *Phys. Fluids* **2007**, *19*, 052103.
143. Cossali, G.; Marengo, M.; Santini, M. Impact of single and multiple drop array on a liquid film. In Proceedings of the 19th Annual Meeting of ILASS, Nottingham, UK, 6–8 September 2004.
144. Ching, B.; Golay, M.W.; Johnson, T.J. Droplet Impacts Upon Liquid Surfaces. *Science* **1984**, *226*, 535–537, doi:doi:10.1126/science.226.4674.535.
145. Leneweit, G.; Koehler, R.; Roesner, K.G.; SchÄFer, G. Regimes of drop morphology in oblique impact on deep fluids. *J. Fluid Mech.* **2005**, *543*, 303–331. https://doi.org/10.1017/S0022112005006476.
146. Zhbankova, S.; Kolpakov, A. Experimental study of collisions of differently sized droplets. *Colloid J. Russ. Acad. Sci.* **1999**, *61*, 390–393.
147. Cheng, M.; Lou, J. A numerical study on splash of oblique drop impact on wet walls. *Comput. Fluids* **2015**, *115*, 11–24.
148. Alghoul, S.K.; Eastwick, C.N.; Hann, D.B. Normal droplet impact on horizontal moving films: An investigation of impact behaviour and regimes. *Exp. Fluids* **2011**, *50*, 1305–1316.
149. Bao, M.L.; Yi, Z.H.; Zhao, D.H.; Liu, H.; Guo, Y.L.; Gong, L.Y.; Shen, S.Q. Dynamic characteristics of oblique droplet impact on a liquid film. *Phys. Fluids* **2025**, *37*, 022101. https://doi.org/10.1063/5.0248681.
150. Stober, J.L.; Santini, M.; Schulte, K. Characterization of splashing and regime thresholds for oblique droplet impact on thin wall films. *Exp. Therm. Fluid Sci.* **2025**, *167*, 111493. https://doi.org/10.1016/j.expthermflusci.2025.111493.

151. Guo, Y.; Lian, Y. Numerical investigation of oblique impact of multiple drops on thin liquid film. *J. Colloid Interface Sci.* **2018**, *530*, 586–594.
152. Okawa, T.; Shiraishi, T.; Mori, T. Effect of impingement angle on the outcome of single water drop impact onto a plane water surface. *Exp. Fluids* **2008**, *44*, 331–339.
153. Liang, G.; Guo, Y.; Yang, Y.; Zhen, N.; Shen, S. Spreading and splashing during a single drop impact on an inclined wetted surface. *Acta Mech.* **2013**, *224*, 2993–3004. https://doi.org/10.1007/s00707-013-0910-6.
154. Roisman, I.V.; Prunet-Foch, B.; Tropea, C.; Vignes-Adler, M. Multiple drop impact onto a dry solid substrate. *J. Colloid Interface Sci.* **2002**, *256*, 396–410.
155. Raman, K.; Jaiman, R.; Lee, T.; Low, H. On the dynamics of crown structure in simultaneous two droplets impact onto stationary and moving liquid film. *Comput. Fluids* **2015**, *107*, 285–300.
156. Li, L.; Jia, X.; Liu, Y.; Su, M. Simulation of double droplets impact on liquid film by a simplified lattice Boltzmann model. *Appl. Therm. Eng.* **2016**, *98*, 656–669. https://doi.org/10.1016/j.applthermaleng.2015.12.050.
157. Liang, G.; Zhang, T.; Chen, H.; Yu, H.; Shen, S. Successive impact of multiple droplets on liquid film. *Eur. J. Mech.—B/Fluids* **2019**, *74*, 389–398. https://doi.org/10.1016/j.euromechflu.2018.09.011.
158. Liang, G.; Zhang, T.; Chen, Y.; Chen, L.; Shen, S. Two-phase heat transfer of multi-droplet impact on liquid film. *Int. J. Heat Mass Transf.* **2019**, *139*, 832–847. https://doi.org/10.1016/j.ijheatmasstransfer.2019.05.055.
159. Liang, G.; Zhang, T.; Yu, H.; Chen, H.; Shen, S. Simultaneous Impact of Multiple Droplets on Liquid Film. *J. Ind. Eng. Chem.* **2018**, *65*, 51–61. https://doi.org/10.1016/j.jiec.2018.04.011.
160. Guo, Y.; Wang, F.; Gong, L.; Shen, S. Numerical study of oblique droplet impact on a liquid film. *Eur. J. Mech.—B/Fluids* **2021**, *85*, 386–396.
161. Gao, Z.; Ding, X.; Song, J.; Chen, J. Analysis of the dynamic behavior of droplet impact on inclined surfaces. *Powder Technol.* **2026**, *476*, 122397.
162. Han, N.; Huang, B.; Sun, B.; He, X. Oblique impacts of nanodroplets upon surfaces. *Langmuir* **2022**, *38*, 13093–13102.
163. Tao, J.; Zhu, H.; Chen, D.; Lin, Z.; Zhu, Z. Heat transfer properties of a droplet colliding with a liquid film on a protruding surface. *Int. J. Heat Mass Transf.* **2025**, *239*, 126574.
164. Zhang, H.; Yu, J.; Zhang, Y.; Wu, S.; Tian, W.; Qiu, S.; Su, G. Study on hydrodynamic characteristics of symmetric two-droplet impact on film using lattice Boltzmann method. *Prog. Nucl. Energy* **2026**, *194*, 106269.
165. Zhou, B.; Jin, Z.; Yang, Z.; Yu, L. Numerical Analysis of Dual Droplet Simultaneous Oblique Impact on a Water Film. *Energies* **2024**, *17*, 2529.
166. Bao, M.; Zhao, D.; Gong, L.; Guo, Y.; Shen, S. Crater radius analysis after dual droplets successive oblique impact on liquid film. *Surf. Interface Anal.* **2024**, *56*, 433–446.
167. Zhou, X.; Wang, H.; Wu, J.; Zhang, Q.; Zhu, X.; Ding, Y.; Chen, R.; Liao, Q. Bounce behaviors of double droplets simultaneously impact cold superhydrophobic surface. *Int. J. Heat Mass Transf.* **2023**, *208*, 124075.
168. Cherdantsev, A.V.; Sinha, A.; Hann, D.B. Studying the impacts of droplets depositing from the gas core onto a gas-sheared liquid film with stereoscopic BBLIF technique. *Int. J. Multiph. Flow* **2022**, *150*, 104033.
169. Cherdantsev, A.; Vozhakov, I. Fast droplets impacting liquid layer under a small angle: A numerical analysis of experimental observations. *Int. J. Multiph. Flow* **2024**, *175*, 104810.
170. Yang, Z.; Zhou, B.; Yang, Z.; Yi, X.; Du, Y.; Jin, Z. Impingement and splashing of a supercooled large droplet on a freezing water film. *Int. J. Multiph. Flow* **2022**, *157*, 104263. https://doi.org/10.1016/j.ijmultiphaseflow.2022.104263.
171. Shen, F.; Fang, W.-Z.; Zhang, S.; Zhang, X.; Yang, C.; Tao, W.-Q. Numerical simulations of freezing behaviors of water droplets impacting cold hydrophobic surfaces. *Appl. Therm. Eng.* **2025**, *258*, 124521.
172. Dash, A.; Sahoo, A.K.; Yadav, A.; Patel, V. Computational modelling of freezing of water droplet impacting on an ice surface. *Mater. Today Proc.* **2021**, *41*, 156–160.
173. Gloerfeld, M.; Schremb, M.; Criscione, A.; Jakirlic, S.; Tropea, C. Impact of supercooled drops onto cold surfaces. In *Droplet Dynamics Under Extreme Ambient Conditions*; Springer: Berlin/Heidelberg, Germany, 2022; pp. 311–332.
174. Zhao, Y.; Wang, J.; Hu, H. An Experimental Study To Characterize Wind-Driven Runback of Water Droplets/Rivulets Over a Flat Surface. In Proceedings of the AIAA SCITECH 2025 Forum, Orlando, FL, USA, 6–10 January 2025.
175. Cossali, G.E.; Marengo, M.; Coghe, A.; Zhdanov, S. The role of time in single drop splash on thin film. *Exp. Fluids* **2004**, *36*, 888–900. https://doi.org/10.1007/s00348-003-0772-0.
176. Myers, T.; Charpin, J.; Thompson, C. Slowly accreting ice due to supercooled water impacting on a cold surface. *Phys. Fluids* **2002**, *14*, 240–256. https://doi.org/10.1063/1.1416186.

177. Vasconcelos, D.; Barata, J.; Silva, A. Splashing correlation for single droplets impacting liquid films under non-isothermal conditions. *Exp. Fluids* **2025**, *66*, 44.
178. Cui, X.D.; Habashi, W.G. A dendritic freezing model for in-flight supercooled large droplets impingement and solidification. *Comput. Fluids* **2023**, *254*, 105778. https://doi.org/10.1016/j.compfluid.2023.105778.
179. Jia, W.; Zhang, F.; Zhang, Z.Q. Numerical and experimental investigation of the supercooled large droplets icing of rotating spinner. *Appl. Therm. Eng.* **2024**, *257*, 124159. https://doi.org/10.1016/j.applthermaleng.2024.124159.
180. Lv, Y.; Hu, Q.; Sun, P.; Shu, L.; Jiang, X. Mechanism of ultrasonic guided wave induced interfacial instability on droplet freezing dynamics. *Appl. Therm. Eng.* **2026**, *293*, 130538.
181. Liu, Y.; Wang, T.; Song, Z.; Chen, M. Spreading and freezing of supercooled water droplets impacting an ice surface. *Appl. Surf. Sci.* **2022**, *583*, 152374.
182. Chang, S.; Yang, Y.; Shi, Q.; Qi, H. Experimental study of shear-driven water film with brightness-based laser-induced fluorescence technique. *Int. J. Multiph. Flow* **2023**, *166*, 104514.
183. Zhu, W.; Shen, Y.; Wang, H.; Zhao, L.; Fu, X.; Jia, Y.; Liu, W.; Liu, S.; Lin, Y.; Jiang, J. Water-Film Flow Characteristics on Surfaces with Diverse Nonwettabilities under Varying Environmental Conditions. *Colloids Surf. A Physicochem. Eng. Asp.* **2025**, *728*, 138602.
184. Miller, D.R.; Potapczuk, M.G.; Bond, T.H. Update on SLD engineering tools development. In Proceedings of the FAA In-flight Icing/Ground De-icing International Conference & Exhibition, Chicago, IL, USA, 16–20 June 2003.
185. Zhang, C.; Liu, H.; Wang, F.; Kong, W. Supercooled large droplet icing accretion and its unsteady aerodynamic characteristics on high-lift devices. *Proc. Inst. Mech. Eng. Part G J. Aerosp. Eng.* **2018**, *232*, 1985–1997.
186. Cui, X.; Habashi, W.G. Numerical Simulation of In-Flight Icing Supercooled Large Droplets Freezing via Smoothed Particle Hydrodynamics. In *Handbook of Numerical Simulation of In-Flight Icing*; Springer: Berlin/Heidelberg, Germany, 2023; pp. 1–48.
187. Elzaabalawy, A.; Meguid, S.A. Multiphysics-multiphase modeling of supercooled droplets impinging superhydrophobic and icephobic surfaces. *Int. J. Multiph. Flow* **2022**, *152*, 104101.
188. Ma, K.; Lin, G.; Jin, H.; Bu, X.; Shen, X.; Wen, D. 3D numerical investigation of surface wettability induced runback water flow behavior. *Renew. Energy* **2025**, *246*, 122937.
189. Ma, L.; Li, H.; Hu, H. An Experimental Study on the Dynamics of Water Droplets Impingement onto a Goose Feather. In Proceedings of the 55th AIAA Aerospace Sciences Meeting, Grapevine, TX, USA, 9–13 January 2017. https://doi.org/10.2514/6.2017-0442.
190. Shang, Y.; Može, M.; Aksoy, Y.T.; Castagne, S.; Seveno, D.; Golobič, I.; Vetrano, M.R. Effect of surface wettability on dynamic behaviors and freezing mechanisms of water droplets impacting cold surfaces. *Phys. Fluids* **2024**, *36*, 092004.
191. Heydarian, S.; Jafari, R.; Momen, G. Recent progress in the anti-icing performance of slippery liquid-infused surfaces. *Prog. Org. Coat.* **2021**, *151*, 106096. https://doi.org/10.1016/j.porgcoat.2020.106096.
192. Daniel, D.; Mankin, M.N.; Belisle, R.A.; Wong, T.-S.; Aizenberg, J. Lubricant-infused micro/nano-structured surfaces with tunable dynamic omniphobicity at high temperatures. *Appl. Phys. Lett.* **2013**, *102*, 231603.
193. Ma, L.; Zhang, Z.; Gao, L.; Liu, Y.; Hu, H. An exploratory study on using Slippery-Liquid-Infused-Porous-Surface (SLIPS) for wind turbine icing mitigation. *Renew. Energy* **2020**, *162*, 2344–2360.
194. Ma, L.; Zhang, Z.; Liu, Y.; Hu, H. An Experimental Study on the Durability of Icephobic Slippery Liquid-Infused Porous Surfaces (SLIPS) Pertinent to Aircraft Anti-/De-Icing. In Proceedings of the 2018 Atmospheric and Space Environments Conference, Atlanta, GA, USA, 25–29 June 2018. https://doi.org/10.2514/6.2018-3654.
195. Islam, A.; Lian, Y. Numerical study of drop impact on slippery lubricated surfaces. *Phys. Fluids* **2023**, *35*, 032115.
196. Cassie, A.; Baxter, S. Large contact angles of plant and animal surfaces. *Nature* **1945**, *155*, 21–22.
197. Farhadi, S.; Farzaneh, M.; Kulinich, S.A. Anti-icing performance of superhydrophobic surfaces. *Appl. Surf. Sci.* **2011**, *257*, 6264–6269.
198. Cao, L.; Jones, A.K.; Sikka, V.K.; Wu, J.; Gao, D. Anti-icing superhydrophobic coatings. *Langmuir* **2009**, *25*, 12444–12448.
199. Nosonovsky, M.; Hejazi, V. Why Superhydrophobic Surfaces Are Not Always Icephobic. *ACS Nano* **2012**, *6*, 8488–8491. https://doi.org/10.1021/nn302138r.
200. Meuler, A.J.; McKinley, G.H.; Cohen, R.E. Exploiting Topographical Texture To Impart Icephobicity. *ACS Nano* **2010**, *4*, 7048–7052. https://doi.org/10.1021/nn103214q.